DEFORMATION OF RUBBER MEMBRANES SUBJECTED TO FLUID LOADINGS

Mei Qiong Shi

October, 2009

Department of Civil Engineering and Applied Mechanics

McGill University, Montréal

Quebec, Canada, H3A 2K6

A thesis submitted to McGill University in partial
fulfillment of the requirements of the degree of
Master of Engineering

ABSTRACT

The mechanical behaviour of a rubber-like elastic material is characterized by its strain energy function, which depends on the type of rubber, including its molecular structure and cross-linking. This thesis presents the results of a series of uniaxial tests that were conducted on natural rubber samples, for the purpose of determining the form of its strain energy function. The simplest model that provides a good match with the stress-strain data is chosen to identify the strain energy function. The validation of the model chosen is performed through an experiment involving fluid loading of a natural rubber membrane that is fixed along a circular boundary. The experimental results of the deformation of the membrane are in good agreement with the values obtained from computational modelling. The studies indicate that the Mooney-Rivlin form of the strain energy function can accurately predict the mechanical behaviour of natural rubber at moderately-large strains.

RÉSUMÉ

Le comportement mécanique des matériaux élastiques comme le caoutchouc est caractérisé par sa fonction d'énergie de déformation, qui dépend du type de caoutchouc, y compris sa structure moléculaire et sa réticulation. Cette thèse présente les résultats d'une série de tests uni-axiaux qui ont été réalisés sur des échantillons de caoutchouc naturel, afin de déterminer sa fonction d'énergie de déformation. Le modèle qui correspond le plus précisément aux données contrainte-déformation est utilisé pour prédire la fonction d'énergie de déformation. La validation du modèle a été faite en réalisant des tests expérimentaux comportant le chargement liquide d'une membrane de caoutchouc naturel qui est fixée le long d'une frontière circulaire. Les résultats expérimentaux de la déformation de la membrane sont en accord avec les valeurs obtenues par la simulation numérique. Les études indiquent que pour les déformations modérées, le modèle d'hyperélasticité Mooney-Rivlin peut prédire avec exactitude le comportement mécanique du caoutchouc naturel.

ACKNOWLEDGEMENTS

TABLE OF CONTENTS

LIST OF TABLES

LIST OF FIGURES

PAPER RESULTING FROM THE RESEARCH

Conference Publication

Shi, M.Q. and Selvadurai, A.P.S. (2009), Mechanical behaviour of a natural rubber, *Proceedings of the CSCE 2009 Annual General Conference*, (L. Lye, Ed.), St John's, Newfoundland, pp. GC-130-1-GC-130-6.

Chapter 1

INTRODUCTION

1.1 Rubber Materials

Natural rubber is obtained via the extraction of latex from a cut made on the bark of a tree. The most popular rubber tree used for commercial purposes is the *Heavea Braziliensis*, originates from South America (Müller and Strehlow (2004)). Other flora species such as *Ficus Elastica*, *Landophia* and *Castilla Elastica* also contain latex, but in lesser quantities. For a long time, natural rubber did not have any commercial potential until the discovery of vulcanization by Charles Goodyear in the 1830s. Uncured natural rubber is sticky and extremely temperature dependent; it easily deforms when slightly heated, and becomes hard and brittle in cool environments. The process of vulcanization modifies the physical properties of the rubber via the cross-linking of the rubber molecules, thus making the material more durable, more resistant to heat and chemical attacks, while maintaining its elasticity at low temperatures. In current usage, the terms *rubber* or *rubber-like* refer to any material that has properties similar to those of natural rubber. The successful developments in this area have led manufacturing and construction industries to adopt rubber for a wide variety of engineering applications including tires, pipes, belts, matting, bridge bearing, inflatable vibration isolation devices, earthquake motion isolation, flood protection structures, biological tissues and landfill liners.

1.2   Literature Review

Problems involving elastic membranes undergoing large deformation have attracted considerable attention over the years. The pioneering work in this area by R.S. Rivlin in

1

the 1940s has formed the basis for the scientific study and technological applications of the theory of hyperelastic materials (see for example the collected works of R.S. Rivlin edited by Barenblatt and Joseph (1997)). Since then, numerous studies have been conducted to validate Rivlin's theory and apply it to a wide range of materials ranging from biological tissues to natural rubber. A great deal of work in the literature is now available on the subject (Spencer (1970); Ogden (1984); Libai and Simmonds (1998); Selvadurai (2006)). The scope of the present work focuses on the loading of a rubber membrane undergoing moderately-large deformations and moderately-large strains; therefore, only problems pertaining to this subject are discussed in more detail.

Membrane loading problems in general are considered very useful in the field of nonlinear elasticity as they allow the development of constitutive equations that model the large deformation behaviour in rubber and elastomeric materials. The first significant analytical study and application of the theory of finite elasticity on the deformation of elastic membranes was carried out by Adkins and Rivlin (1952), using the neo-Hookean and Mooney forms of the strain energy function. These authors gave several mathematical solutions to different axially symmetric problems. A summary of their work including more recent ones are given by Green and Adkins (1970). The inflation of pre-stretched uniform circular rubber membranes was studied by Hart-Smith and Crisp (1967) and Klingbeil and Shield (1964). Their experimental results were similar to Treloar's results for large extensions obtained by using more complicated forms for the strain energy function. Vaughan (1980) performed similar experiments where a finitely stretched circular membrane was inflated into a shallow bowl. Kydoniefs and Spencer (1967; 1969), looked into the problem of slow inflation of a closed cylindrical membrane under internal pressure and obtained an exact solution for the Mooney material. Dickey (1967; 1983) performed many experiments on circular membranes under normal pressure and found axisymmetric solutions for these problems using a numerical integration scheme. He also derived an exact theory for the problem of a circular membrane subjected to a vertical pressure, confirming Föppl theory. Alexander (1971) studied the effect of instability of an inflated cylindrical membrane under axial loading using a special form of strain energy function. Wu (1971) investigated contact problems of

2

inflated cylindrical membranes with a life raft as an example. Benedict et al. (1979) analyzed the simultaneous extension and inflation of membranes using an exponential form of a strain energy function. Needleman (1977) examined the inflation of a slightly imperfect spherical rubber balloon, in which the axisymmetric equilibrium is determined using the Ritz-Galerkin procedure. He quotes earlier works done by Feodosev (1968) and Shield (1972) who have used the same procedure to solve imperfect spherical balloons. Haughton (1980) continued in this area and studied both perfect and imperfect cases of membrane inflation. Feng and Yang (1970) examined several problems including the free and confined inflation of a flat circular membrane. Using a strain energy function of the Mooney-Rivlin type, they provided numerical solutions to the inflation of a flat membrane, longitudinal stretching of a tube, and flattening of a hemispherical cap. More experiments conducted by these authors on inflation and inflation-induced contact problems related to both circular and rectangular membranes are given by Feng and Yang (1970), Yang and Lu (1973), Feng et al. (1974), and Feng and Huang (1975). Feng and Yang (1973) investigated gas-filled spherical membranes of Mooney material to which additional loads are applied. One experiment consisted of compressing the inflated spherical membranes between two rigid plates and another indented by rigid disks. Lardner and Pujara (1980) extended the experiments and analysis with liquid-filled membranes. Wineman et al. (1979) performed membrane inflation experiments and showed how the measured profiles and stretch ratio distribution of a material can be used to determine the precise form of the strain energy function. Weinitschke (1980) extended his previous work (1970) on circular membranes and performed a series of experiments involving an annular membrane under normal pressure for different boundary conditions. Weinitschke (1987) also provided detailed analyses of an annular elastic membrane under surface and edge loads. Grabmüller and Weinitschke (1986) and Grabmüller and Novak (1988) examined similar problems and used integral equation methods to confirm Föppl and Reissener theories. Matsikoudi-Iliopoulou and Lianis (1982) studied the asymmetric deformation of membranes with torsion and came up with analytical solutions for that problem. Matsikoudi-Iliopoulou (1987) then combined his earlier findings to generate a solution for the deformation of a pressurized cylindrical membrane reinforced with one family of inextensible fibers. Kelkar et al.

3

(1985) examined the problem of a circular membrane with fixed peripheral edges. Using a finite difference technique, they studied the displacement and stresses in the material under three different loading conditions. Beatty (1987) discussed several features for the inflation of a spherical balloon, including the non-uniqueness and instability of elastic membranes. Khayat et al. (1992) and Khayat and Derdouri (1995) examined the inflation of neo-Hookean cylindrical membranes subjected to pressure and axial stretching. Chen and Cheng (1996) looked into ponding problems where ponding pressures were acting on a circular membrane due to the weight of a liquid filling the area created by the deflection of the membrane. They used an iterative technique to solve for the loaded and unloaded portions of the membrane. Tuan (1998) also analysed ponding of circular membranes using a fourth-order Runge-Kutta method. He found good agreement between his finite element simulations and his experimental results. Verron et al. (1999) analysed the inflation of a spherical membrane under dynamic conditions using the neo-Hookean model. Przybylo and Arruda (1998) and Li et al. (2001) worked on the inflation of circular membranes to determine properties of elastomers and polymeric materials, respectively. The inflation of planar circular viscoelastic membranes has been studied by various authors: Wineman (1976) performed several inflation tests on styrene-butadiene rubber, Feng (1992) considered latex rubber membranes and Hassager et al. (1999) looked into the inflation and instability of a polymeric fluid membrane using the Doi-Edwards and Tom-Pom models. Wineman (1978) also developed a numerical program for the analysis of simultaneous axial stretching and inflation of a tubular membrane, using the BKZ model. More recently, Wineman (2007) looked into the inflation of nonlinear viscoelastic circular membrane and the extension and inflation of a circular tube. He presents his numerical solutions that combine nonlinear elasticity with Volterra integral equations. Katsikadelis and Nerantzaki (2002; 2003) looked into the deformations of elastic and floating membranes of arbitrary shape under partial and full ponding loads. Colombi (2006) investigated the ponding problem on flat steel roof grids. Nerantzaki and Kandilas (2007) analysed the deformation of membranes containing rigid inclusions for different loading pattern. Liu and Rahn (2003) presented experimental results conducted on cylindrical elastic membranes under inner pressure and axial load for two families of inextensible fibers. David and Humphrey (2004) and Mori et al.

(2005) have recently looked into the problem of circular holes in membranes for analysing the effects of cavities in thin tissues during clinical procedures. Scott et al. (2004) used annular membrane models to perform spherical indentation tests on circular elastomeric films. Begley and Mackin (2004) presented their experimental and numerical results of a spherical indentor on freestanding circular thin films. Selby and Shannon (2009) looked into the problem of inflating a circular elastomeric membrane into a horizontally semi-infinite liquid reservoir.

This overview is far from being complete; the review article by Beatty (1987) and the volumes by Green and Adkins (1970), Truesdell and Noll (1992) and Libai and Simmonds (1998) provide many references to topics of interest to the membrane problems.

1.3   Objectives and Scope of Thesis

The current work examines the mechanical behaviour of natural rubber at moderately-large strain (0-100% engineering strain). A series of uniaxial tests were performed on the rubber sample to determine what type of energy function can be used to describe its mechanical response. Numerous strain energy functions exist; attention will be focused on Mooney-Rivlin, neo-Hookean and Ogden models. The simplest model that provides the best match for the stress-strain data was chosen to model the mechanical behaviour of the natural rubber material. The validation of the parameters was done through an experiment involving fluid loading on a gum rubber membrane that was fixed along a circular boundary. The membranes used have diameters of 146 mm and thicknesses of 0.794 mm and 1.588 mm. The deflected profiles of the membrane at various pressures were recorded and the results compared with finite element simulations. The finite element analysis software ABAQUS was used to perform the computational simulations. For the isothermal hyperelastic models considered, the material is assumed to be incompressible. The mechanical behaviour of the natural rubber is elastic and strain-rate independent during quasi-static deformations. Finally, a comparison of experimental and

numerical results of the response of the membrane under fluid loading was conducted to validate the choice of the hyperelastic model and its parameters.

Chapter 2

MECHANICAL BEHAVIOUR OF RUBBER

2.1 Non-Linear Elasticity

According to ASTM D1566-06 (ASTM (2006)), rubber is defined as a material that is capable of recovering from large deformations quickly and forcibly, and can be, or already is, modified to a state in which it is essentially insoluble (but can swell) in boiling solvent. Rubbers possess a number of unique material properties such as a low elastic modulus, a low thermal conductivity, little or no hysteresis, a high percentage of elongation (in the range of 500% to 1000% engineering strain) before fracture, and almost no volume change during deformation. Rubber-like materials are characterized by hyperelastic deformability and exhibit a stress-strain curve in tension that is non-linear. Consequently, Hooke's law is not applicable; it is not possible to assign a definite value to Young's modulus except in the region of small strains, where the Young's modulus is of the order of 1.0 MPa compared to typical hard solids where the Young's modulus is in the region of 10^4-10^5 MPa and have a corresponding maximum elastic extensibility of less than 1.0%. A typical stress-strain curve for a natural rubber is shown in Figure 2.1.
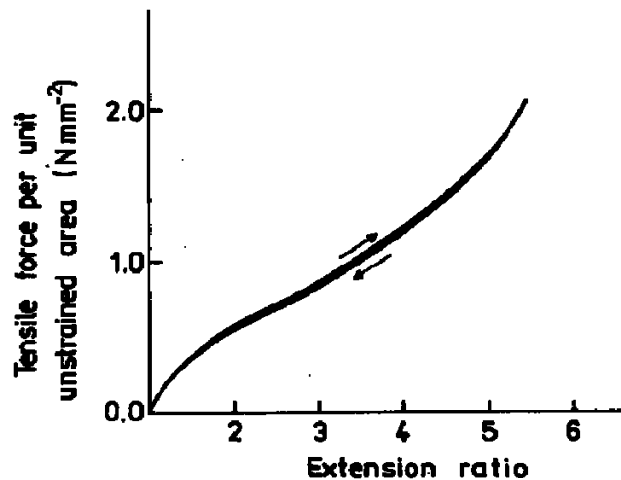
Figure 2.1 The stress-strain curve of a typical incompressible hyperelastic material (Treloar, 1975)

2.2 Hysteresis and Mullins Effect

Hysteresis occurs when the unloading path of the stress-strain curve differs from the loading path. Very few elastomers, such as natural rubber and some grades of polyurethane, show hysteretic behaviour. In the case of natural rubber, previous tests by Selvadurai (2006) showed that the loading and unloading paths are practically identical at low strains (Figure 2.2). Hysteresis, however, becomes more apparent at large strains. For instance, in the case of geosynthetic materials, Yu (2005) showed that the loading stress-strain path differs significantly from its unloading path (Figure 2.3).

Figure 2.3 shows that a *strain-induced stress softening* phenomenon is present. This phenomenon, also called the *Mullins effect*, was named after L. Mullins for his numerous studies on the behaviour of unfilled and filled rubbers during the 1950s and 1960s (Mullins and Tobin (1957; 1965); Mullins (1969)). The significant reduction in stress at a given strain level during unloading compared to the stress on initial loading on the first and successive cycles is characteristic of the *Mullins effect*. Unfilled rubber generally exhibits stress-softening at high strains, while filled rubber demonstrates substantial stress-softening at relatively low strains.
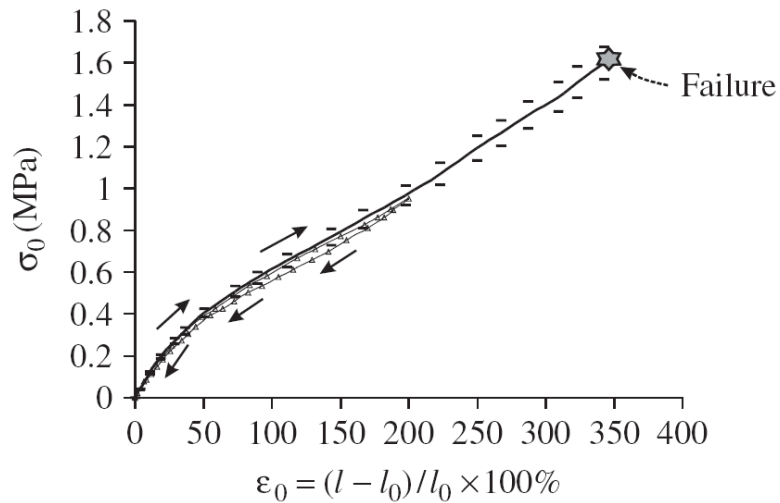
Figure 2.2   Stress-strain curve for a natural rubber specimen in uniaxial tension (Selvadurai, 2006)
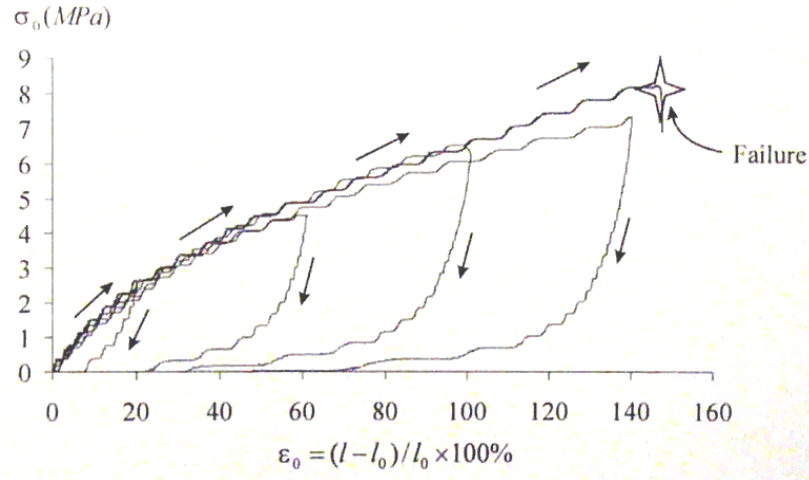
Figure 2.3 Stress-strain curve for PVC geosynthetic specimen in uniaxial tension (Yu, 2005)

2.3   Crystallization

Unstrained vulcanized rubber is known to be amorphous at room temperature, but can produce immediate crystallization when subjected to rapid high extension. A simple experiment conducted by Müller and Strehlow (2004) shows the crystallization phenomenon: a thin strap of natural rubber was rapidly stretched up to 8 times its original length. Internal heating of the rubber made the temperature of the material rise from 20°C to 45°C. On unloading from the stretched state (before it had time to cool), the rubber specimen returned completely to its original condition. However, when the rubber strap was held in its stretched state until it cooled down to 20°C before release, it remained stretched in a stress-free configuration; the rubber has undergone crystallization. If the stretched sample is then heated to 45°C, it experiences a shape recovery and returns to its original state.

In this work, the rubber experiences quasi-static loading, which is known to generate a negligible heat and stretching.   In this study, internal heating effects such as crystallization are disregarded.

9

2.4   Large Elastic Deformation and Stress-Strain Relation

When a material body undergoes a deformation, the measurement of its displacement and deformation in space is of interest to continuum mechanics. A large amount of literature is available on materials that undergo large deformation (e.g. Rivlin (1960); Green and Adkins (1970); Spencer (1970); Ogden (1984; 2004)) and only a summary on the relevant points will be given here. For a material point, P, let $\mathbf{X}_A (A = 1,2,3)$ be the reference position vector with respect to the initial coordinate system $\hat{e}_A (A = 1,2,3)$, and $\mathbf{x}_i (i = 1,2,3)$ be the new position vector with respect to the deformed coordinate system, $\hat{e}_i (i = 1,2,3)$. The new position of point P is now defined as P' (Figure 2.4).
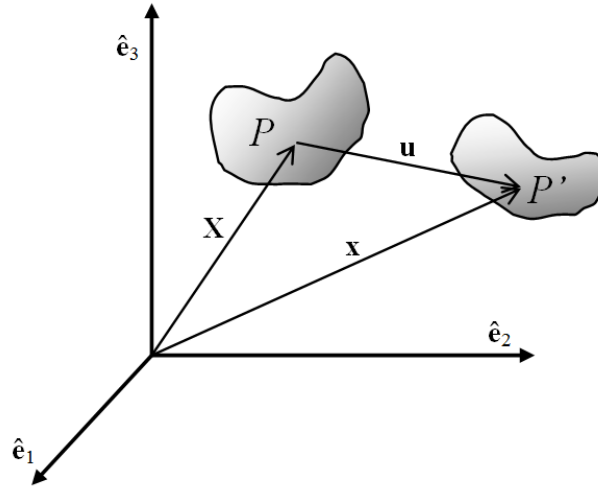
Figure 2.4   Motion of a continuum body in space with displacement vector $\mathbf{u}$ and
position vectors $\mathbf{X}$ and $\mathbf{x}$, defining points P and P', respectively

The relationship between the reference position vector, $\mathbf{X}$, and the new position vector corresponding to the deformed configuration, $\mathbf{x}$, is given by the displacement vector, $\mathbf{u}$, expressed as

$$u_i = x_i - X_A \tag{2.1}$$

The constitutive equations which characterize the elastic solid as a material are presented below. It is defined as a material in which its components of stress are single-valued functions of the deformation gradients, so that

$$\sigma_{ij} = \phi_{ij}(f_{RA}) \tag{2.2}$$

where f_{RA} are components of the deformation gradient tensor

$$f_{RA} = \partial x_R / \partial X_A \tag{2.3}$$

Using matrix notation,

$$\boldsymbol{\sigma} = \| \sigma_{ij} \|, \quad \mathbf{F} = \| f_{RA} \|, \quad \boldsymbol{\phi} = \| \phi_{ij} \|, \tag{2.4}$$

equation (2.2) takes the form

$$\boldsymbol{\sigma} = \boldsymbol{\phi}(\mathbf{F}). \tag{2.5}$$

The *right Cauchy-Green tensor*, **C**, is obtained from the deformation gradient and has the following form

$$\mathbf{C} = \mathbf{F}^{\mathbf{T}}\mathbf{F} \quad ; \qquad C_{ij} = f_{Ri} f_{Rj} = \frac{\partial x_R}{\partial X_i} \frac{\partial x_R}{\partial X_j}. \tag{2.6}$$

For isotropic elastic materials, the Cauchy stress tensor $\boldsymbol{\sigma}$ only depends on the *left Cauchy-Green strain tensor*, **B**, given by

$$\mathbf{B} = \mathbf{F}\mathbf{F}^{\mathbf{T}} \quad ; \qquad B = \| g_{ij} \| \quad ; \quad g_{ij} = f_{iR} f_{jR} = \frac{\partial x_i}{\partial X_R} \frac{\partial x_j}{\partial X_R}. \tag{2.7}$$

The invariants of **B** can be expressed in terms of the principal stretches $\lambda_i (i = 1,2,3)$ as follows

$$I_1 = g_{ii} = \lambda_1^2 + \lambda_2^2 + \lambda_3^2$$

$$I_2 = \frac{1}{2}(g_{ii}g_{jj} - g_{if}g_{ij)} = \lambda_1^2\lambda_2^2 + \lambda_2^2\lambda_3^2 + \lambda_3^2\lambda_1^2 \tag{2.8}$$

$$I_3 = \lambda_1^2\lambda_2^2\lambda_3^2$$

It can be shown (Rivlin (1960); Spencer (1970)) that the constitutive relationship for an incompressible isotropic elastic material undergoing large strain can be represented in the generalized form

$$\boldsymbol{\sigma} = -p\mathbf{I} + \phi_1\mathbf{B} + \phi_2\mathbf{B}^2 \tag{2.9}$$

11

where p is an arbitrary scalar pressure, $\mathbf{I}$ is the unit matrix and ϕ_1 and ϕ_2 are functions of the invariants I_1 and I_2. If a strain energy function $W(I_1, I_2)$ exists, then ϕ_i can be expressed in terms of W.

2.5 Strain Energy Function

The relationship that assumes the existence of a strain energy as a function of the invariants was first published by Mooney (1940) then confirmed by Rivlin (1948). The strain energy function relates the energy stored in an elastic material to its strain or elongation components. It is normally referred to as W and is expressed as an isotropic function of its three invariants of the principal stretches:

$$W = f(I_1, I_2, I_3) \tag{2.10}$$

where I_1, I_2 and I_3 are related to the three principal stretch ratios λ_1, λ_2 and λ_3 (equation (2.8)) . The values of λ_i are given by $(1 + \varepsilon_i)$ where ε_i is the corresponding principal extension. In the special case of the membrane material that was used in the research, it was found that $I_3 \approx 1$ (experimental data to support this will be presented in a subsequent chapter). As a result, the third principal strain changes to the following when the strains of λ_1 and λ_2 are applied in the x_1 and x_2 directions of an incompressible material:

$$\lambda_3 = \frac{1}{\lambda_1 \lambda_2}. \tag{2.11}$$

The three invariants may therefore be expressed in terms of two principal stretch ratios,

$$
\begin{aligned}
I_1 &= \lambda_1^2 + \lambda_2^2 + \frac{1}{\lambda_1^2 \lambda_2^2} \\
I_2 &= \lambda_1^2 \lambda_2^2 + \frac{1}{\lambda_1^2} + \frac{1}{\lambda_2^2} \\
I_3 &= 1
\end{aligned}
\tag{2.12}
$$

and the strain energy density function is further reduced to a function of two variables,

$$W = f(I_1, I_2). \tag{2.13}$$

2.6 Constitutive Models

Several constitutive models have been developed over the years to describe the hyperelastic response of rubber-like materials. The pioneering work in this area by R.S. Rivlin in the 1940s has formed the basis for the scientific study and technological applications of the theory of hyperelastic materials (see for example Barenblatt and Joseph (1997)). Treloar (1944) has made significant contributions to the study of hyperelastic materials with a number of important publications on experimental work on rubber-like materials. He developed a model based on molecular theory, where the energy stored in the rubber takes the following form:

$$W = \frac{1}{2}G(\lambda_1^2 + \lambda_2^2 + \lambda_3^2 - 3) = \frac{1}{2}G(I_1 - 3),\tag{2.14}$$

where G is the linear elastic shear modulus. Also G can be expressed in the form of $G = NkT$, where N is the number of chains of molecules per unit volume, k is Boltzmann's constant ($1.381 \times 10^{-23} J/K$), T is the absolute temperature and λ_1, λ_2 and λ_3 are the principal stretch ratios. This form of the energy function also referred to as the neo-Hookean model of hyperelasticity has been used extensively due to its simplicity, having only one independent material constant.

The above form of energy function was based on a paper by Mooney (1940). Mooney developed a phenomenological theory around the same time as the early development of the statistical theory. He assumed the material to be homogeneous, isotropic, elastic, incompressible, and obeys Hooke's Law in pure shear, which states that the shear strain is directly proportional to the shear stress. Mooney provided a more complete molecular model that contained two material parameters (Mooney (1940)):

$$W = \frac{G}{4}\sum_{i=1}^{3}\left(\lambda_i - \frac{1}{\lambda_i}\right)^2 + \frac{H}{4}\sum_{i=1}^{3}\left(\lambda_i^2 - \frac{1}{\lambda_i^2}\right).\tag{2.15}$$

It can be seen that equation (2.14) is a special case of (2.15) and is obtained when $H = 0$.

A simpler form of energy function was later proposed by Rivlin, who performed many experimental and theoretical studies during the period from 1948 to 1955 based on Mooney's model. Rivlin's general form of the strain energy function is given by

$$W = \sum_{i,j=0}^{\infty} C_{ij} (I_1 - 3)^i (I_2 - 3)^j \tag{2.16}$$

where C_{ij} are material constants and I_1 and I_2 are the principal strain invariants. It is noted that when $i = j = 1$, this generalized model gives the first-order Mooney-Rivlin model, where the first two terms are

$$W = C_1 (I_1 - 3) + C_2 (I_2 - 3) . \tag{2.17}$$

Higher order strain energy functions exist, but they are not practical because the experimental evaluation of the large number of coefficients is difficult to achieve. Yeoh (1997) and Gent (1997) observed that rubber-like materials are not sufficiently reproducible to accurately determine the higher order strain energy functions. The Mooney-Rivlin model allows the constants to be determined experimentally, relatively conveniently. As a result, the Mooney-Rivlin model has become the most widely used strain energy function for rubber-like materials undergoing moderately large strains (Selvadurai (2006)). For the special case of uniaxial loading of a rubber specimen, using the Mooney-Rivlin model, the stress-strain equation can be expressed as

$$\sigma_0 = 2 \left(C_1 + \frac{C_2}{\lambda} \right) \left(\lambda - \frac{1}{\lambda^2} \right) \tag{2.18}$$

where the nominal stress, σ_0, defined as the load over the current area, is related to the uniaxial stretch in the test direction, λ. Rearranging, (2.18) becomes

$$\frac{\sigma_0}{2(\lambda - \lambda^{-2})} = C_1 + \frac{C_2}{\lambda} . \tag{2.19}$$

The above equation, which can be plotted as $\sigma_0 / 2(\lambda - \lambda^{-2})$ vs. λ^{-1}, is referred to as a Mooney-plot. For a hyperelastic rubber material, the Mooney plot gives a straight line, with a slope of C_2 and the intercept (as $1/\lambda \to 0$) gives the value of C_1. More details about the Mooney-plot and ways to obtain the coefficients are discussed in section 3.4.

Many other hyperelastic models exist, with Ogden's model being the second most widely used. The model proposed by Ogden (1972; 1984) expresses the strain energy function in terms of the principal stretch ratios rather than the strain invariants. Ogden (1972) used Treloar (1975) results to develop this model. This model has shown good agreement with experimental results for large strains of the order of 300%, and can be used for both incompressible and compressible hyperelastic materials. The form for the strain energy function proposed by Ogden (1972) is given by

$$ W = \sum_{i=1}^{N} \frac{2\tilde{\mu}_i}{\alpha_i^2} (\lambda_1^{\alpha_i} + \lambda_2^{\alpha_i} + \lambda_3^{\alpha_i} - 3) \tag{2.20} $$

where $\sum_{i=1}^{N} \tilde{\mu}_i = G$ (the linear elastic shear modulus) and N, $\tilde{\mu}_i$, α_i are the material parameters. The result (2.20) reduces to the neo-Hookean model when $N = 1$, $\alpha_1 = 2$ and $\mu_1 = NkT$. Also, assigning $N = 2$, $\alpha_1 = 2$, $\mu_1 = 2C_1$, $\alpha_2 = -2$, $\mu_2 = 2C_2$ to Ogden's model, we obtain the first-order Mooney-Rivlin model (Equation (2.17)).

The model developed by Yeoh (1993) represents the elastic properties of rubber by assuming that the strain energy function is independent of the second strain invariant,

$$ W = \sum_{i=1}^{N} \tilde{C}_i (I_1 - 3)^i , \tag{2.21} $$

where $\tilde{C}_i$ are constants. In the special case where $N = 1$, the Yeoh model reduces to the neo-Hookean model.

Many other constitutive models exist, including Blatz and Ko (1962), Hart-Smith (1966), Oden and Sato (1967), Christensen (1980), Flory and Erman (1982), Arruda and Boyce (1993) and Gent (1996). In-depth reviews of these models can be found in Deam and Edwards (1976), Ogden (1982), Boyce and Arruda (2000), and Saccomandi and Ogden (2004). Their applicability to rubber-like materials undergoing moderately-large strains was recently investigated by Selvadurai (2006).

Chapter 3

UNIAXIAL TESTING OF NATURAL RUBBER

3.1 Measurement of the Mechanical Properties

The mechanical properties of vulcanized rubber were determined from uniaxial tensile tests. The testing facility consisted of a servo-controlled MTS Machine equipped with a load cell with a capacity of 150 kN. The Advantage™ Wedge Action Grips available in the Material Testing Laboratory of the Department of Civil Engineering and Applied Mechanics of McGill University were used for the experiment since they have knurled clamping plates that provide good fixity at the ends of the specimen. The details of the experimental setup and of the grips are shown in Figure 3.1 and 3.2, respectively. The tests involve the stretching a rubber strip specimen attached to the upper and lower set of grips. The lower set of grips is fixed during testing while the upper set moves either upwards or downwards in a displacement-controlled mode. The speed of movement of the cross-head during testing is controlled at a quasi-static strain rate of 20%/min. A special highly sensitive low capacity load cell (2224 N (500 lbs)) was used in the testing machine since the forces measured during uniaxial testing were very small compared to the peak load capacity of the MTS machine. Technical specifications of the load cell are presented in section 4.4. Two special adaptors were added to the initial setup in order to effectively attach the load cell to the MTS Testing frame.

Figure 3.1   The test facility
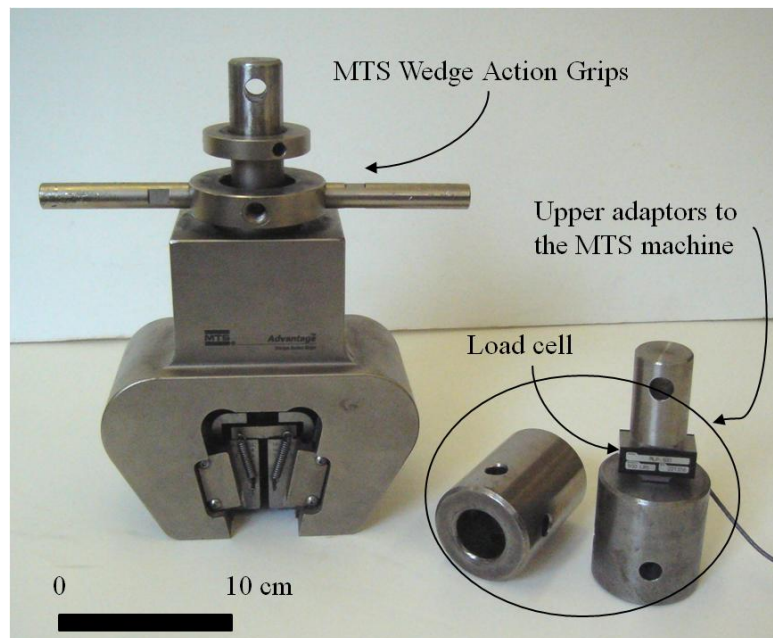
(a) Upper set of grips
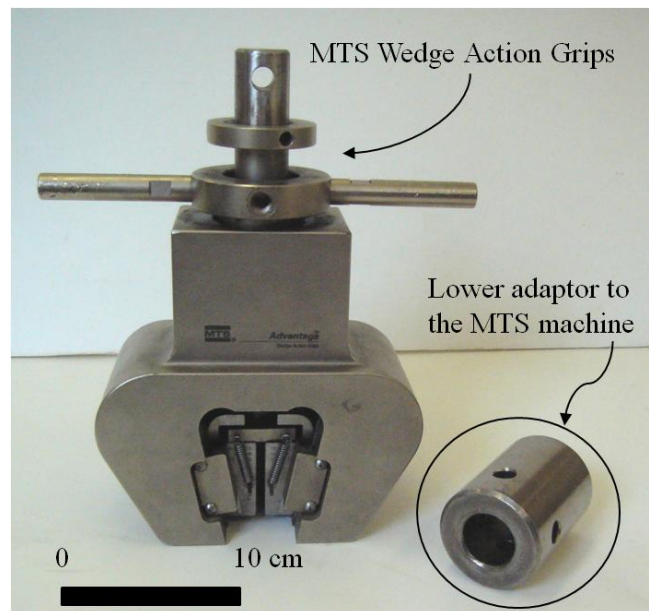
(b) Lower set of grips

Figure 3.2   Details of the set of grips

To prevent any slippage between the specimen and the plates of the Advantage™ Wedge Action Grips, an additional layer of gum rubber was bonded to each end of the test specimen, using a non-reactive Krazy Glue® instant adhesive (Figure 3.3). This extra layer increased the thickness of the ends of the gum rubber specimen, which was then tightly clamped between the two knurled plates of the Wedge Action Grips. It was observed previously that slippage occurred without this additional layer (Selvadurai (2006); Selvadurai and Yu (2006)). Tests indicated that without the additional layer, slippage would be limited at small strains but become noticeable at moderate and large strains, primarily due to the progressive friction loss (associated with a Poisson-type contraction) between the membrane and the clamping system during stretching. There is the possibility of chemical reaction between the instant adhesive and the rubber specimen if the testing takes place over a long period; however, since the tests on the rubber specimens were performed within one hour of the adhesive application, the effects of any chemical reaction were disregarded. Six rubber specimens of two different thicknesses were tested. All samples were cut from the same sheet to minimize any batch-to-batch variation. The specimens used measured 150 mm x 30 mm in profile with an initial cross section of 30 mm x 0.794 mm and 30 mm x 1.588 mm. A typical specimen is shown in Figure 3.4. The stress-strain data collected from the experiments are presented in terms of engineering stress and engineering strain. The engineering stress, S, is defined as the applied load, P, divided by the unstrained cross-sectional area, A_0. The engineering strain, ε, is defined as the change in length, ($\Delta L = L - L_0$), divided by the original length, L_0, and the extension or stretch ratio, λ, is the current length, L, divided by the original length. In the experiments performed, the original length was taken as the distance between two edges of the specimen ($L_0 = 150$ mm) as indicated in Figure 3.4. The strain was calculated as the percentage change of the original length. The results of the uniaxial tests conducted up to a strain of 100 % are presented in section 3.2.

The experiments were conducted in the Materials Testing Laboratory where the room temperature was approximately 24°C. The duration of each tensile test was approximately 35 minutes and during this period the temperature in the laboratory

fluctuated by less than 1°C. It can be assumed that the temperature fluctuations had virtually no effect on the change in the mechanical properties of the natural rubber.

Figure 3.3   Krazy Glue instant adhesive
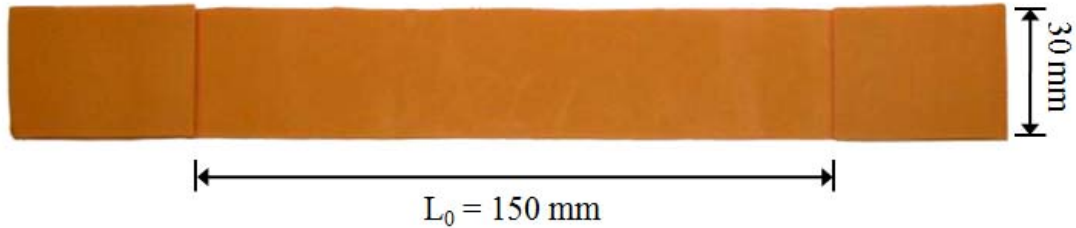
Figure 3.4   Specimen prepared for tensile testing

3.2   Uniaxial Tests Results

The results of the uniaxial tests conducted on natural gum rubber of thicknesses 0.793mm and 1.588 mm are shown in Figure 3.5. The natural gum rubber undergoes moderate strains, i.e. up to 100% strain, during the tensile test. Due to the height limitation of the MTS machine, the material could not be tested up to failure; however, natural rubber is known to fail at a strain in the range of 800% – 1000% (Treloar (1975)). The results show good repeatability between each set of experiments, and within the range of accuracy of the tests. From the loading-unloading stress-strain curves shown in Figure 3.5, it can be observed that hysteresis was negligible, especially for the thinner specimen. The unloading behaviour of the gum rubber follows relatively closely the loading curve and the material does not display any significant irreversible deformation. Other hyperelastic materials, such as PVC geosynthetic, exhibit creep and irreversible strains

during uniaxial testing (Yu (2005)). Natural rubber also has the advantage of being strain-rate independent. Results of uniaxial tests conducted at three different strain-rates, 20%/min, 40%/min and 60%/min, indicated that the strain rate has no significant influence on the stress-strain behaviour of the material.
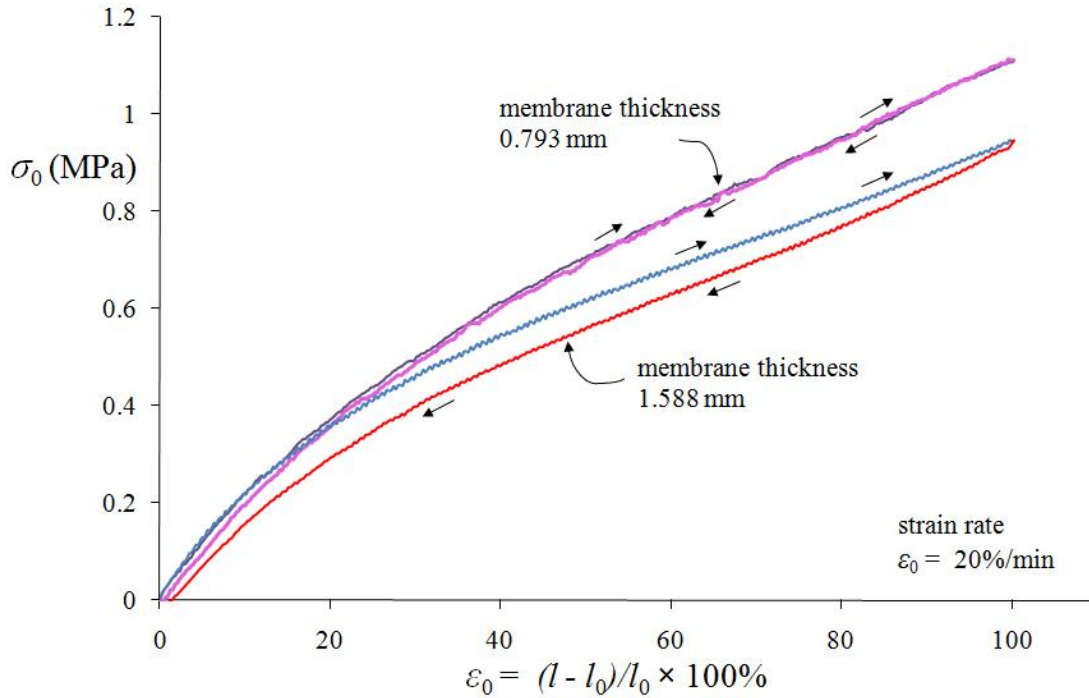
Figure 3.5   Stress-strain response of a rubber strip to uniaxial stretching

Additional strain data can be extracted from selected points in the continuous stress-strain curve shown in Figure 3.6a. During tensile testing, the specimen should produce a homogeneous deformation. The homogeneity of the deformation is a requirement for the data analysis procedures which rely on the appropriate measures of stress and homogeneous strain. However, in reality, it is practically impossible to achieve perfect homogeneity of the specimen during stretching. Since the ends are gripped, the prevention of lateral contraction leads to non-homogeneity in the strain field. To examine the extent to which the end constraints influence the development of homogeneous straining, a comparison between the physical stretching of the specimen

and the relative extension of the grips was made. The procedure used was identical to that given in Selvadurai (2006). A grid was drawn on the rubber specimen using a fine black marker with spacings of 10 mm and 30 mm between gridlines. As the sample stretched, the horizontal gridlines were used to calculate the real physical length for different sections on the rubber specimen (Figure 3.6b). A 5 Megapixels digital camera captured the deformed configuration of the specimen at different strain ranges. The distance between the horizontal gridlines was first measured in image *pixels*, and then calibrated against a known physical distance. The known physical distance was chosen as the distance between the two grips. The real distance at different extensions can then be obtained via a conversion between the image *pixels* and the known physical distance. Figure 3.6b shows the strains measured at different sections of the specimen. Test results indicate that the effects of the fixity constraints give errors of 3.4%, 1.5% and 0.2% at average strains in the range of $\varepsilon_0 = 27\%$, 54% and 81%, respectively.

σ_0 (MPa)

$\varepsilon_0 = 20\%/min$

150mm

30mm

Undeformed specimen

strain rate
$\varepsilon_0 = 20\%/min$

$\varepsilon_0 = (l - l_0)/l_0 \times 100\%$

(a) Stress-strain curves

25%
26%
27%
26%

56%
54%
53%
54%

81%
81%
80%
81%
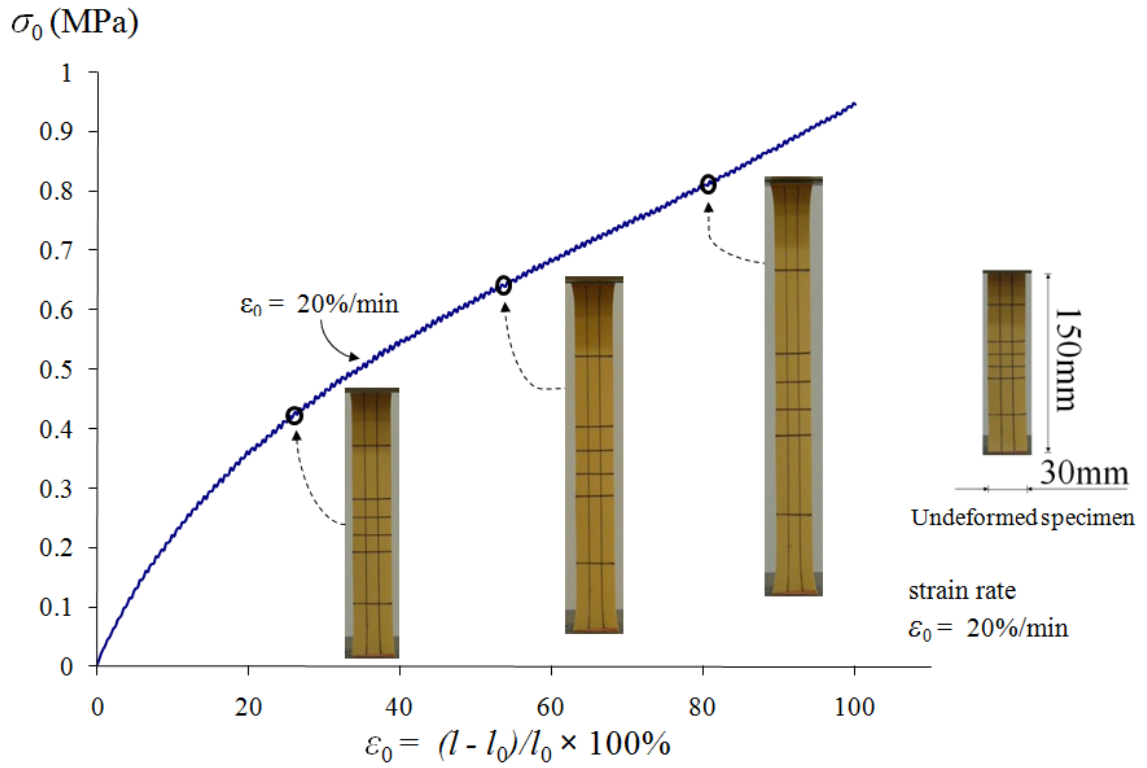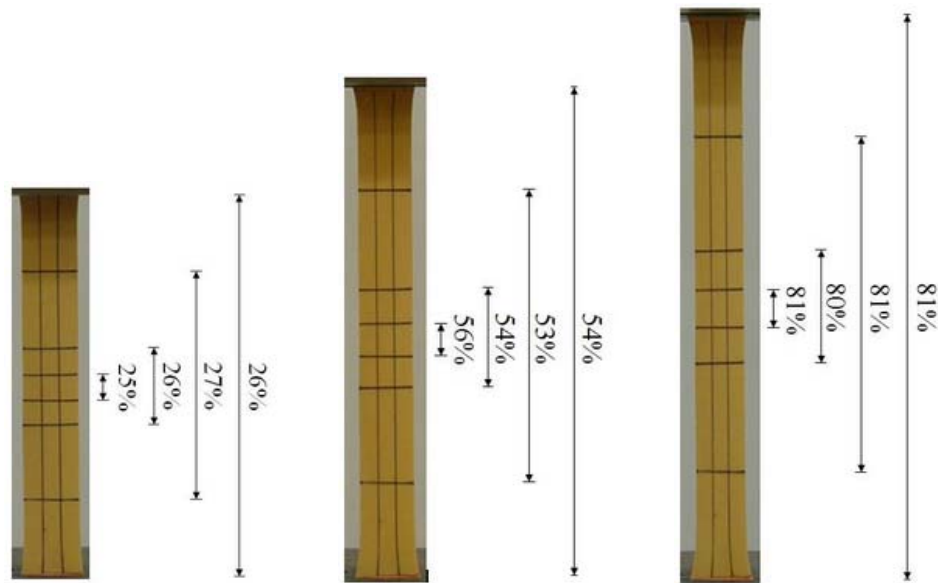
(b) Deformed shapes with strain measured at different sections of the specimen

Figure 3.6   Tensile behaviour of natural rubber strips (membrane thickness: 1.588 mm)

23

3.3 Constitutive Modelling Results

In this section we use the uniaxial test data to identify the parameters associated with the neo-Hookean, Mooney-Rivlin and Ogden models and proceed to choose the simplest model that provides the best match for the stress-strain data in the selected range of strains. The easiest way to obtain the coefficients is to use the curve-fitting hyperelastic models supplied by most Finite Element Analysis (FEA) software. In this study, the commercial FE software ABAQUS (ABAQUS/Standard (2008)) was used for both modelling and calculations. ABAQUS contains a large library of hyperelastic models designed for rubber materials, namely: polynomial, Mooney-Rivlin, reduced polynomial, neo-Hookean, Yeoh, Arruda-Boyce, Ogden and Van der Waals. The Mooney-Rivlin and reduced polynomial models are particular forms of the polynomial model. The neo-Hookean and Yeoh models are special cases of the reduced polynomial model. ABAQUS allows the evaluation the hyperelastic material behaviour by automatically creating response curves using selected strain energy potentials (Figure 3.7). ABAQUS allows the input of either uniaxial tension data, or equi-biaxial extension data, or planar tension data, or any combination of these loading states to be used for parameter/ model identification. Although the ABAQUS manuals suggest that the input of data obtained from multi-stress states will optimize the accuracy of hyperelastic model predictions, only uniaxial tension test data were used in this study to determine the material coefficients. It was assumed that the planar and biaxial tension tests could be omitted without compromising accuracy. Each parameter was determined using the least squares method. Figure 3.8 shows a comparison of the modelling of the tensile behaviour of the natural rubber material obtained using different forms of the strain energy function. It can be observed that the Mooney-Rivlin model provides the closest fit to the experimental data.
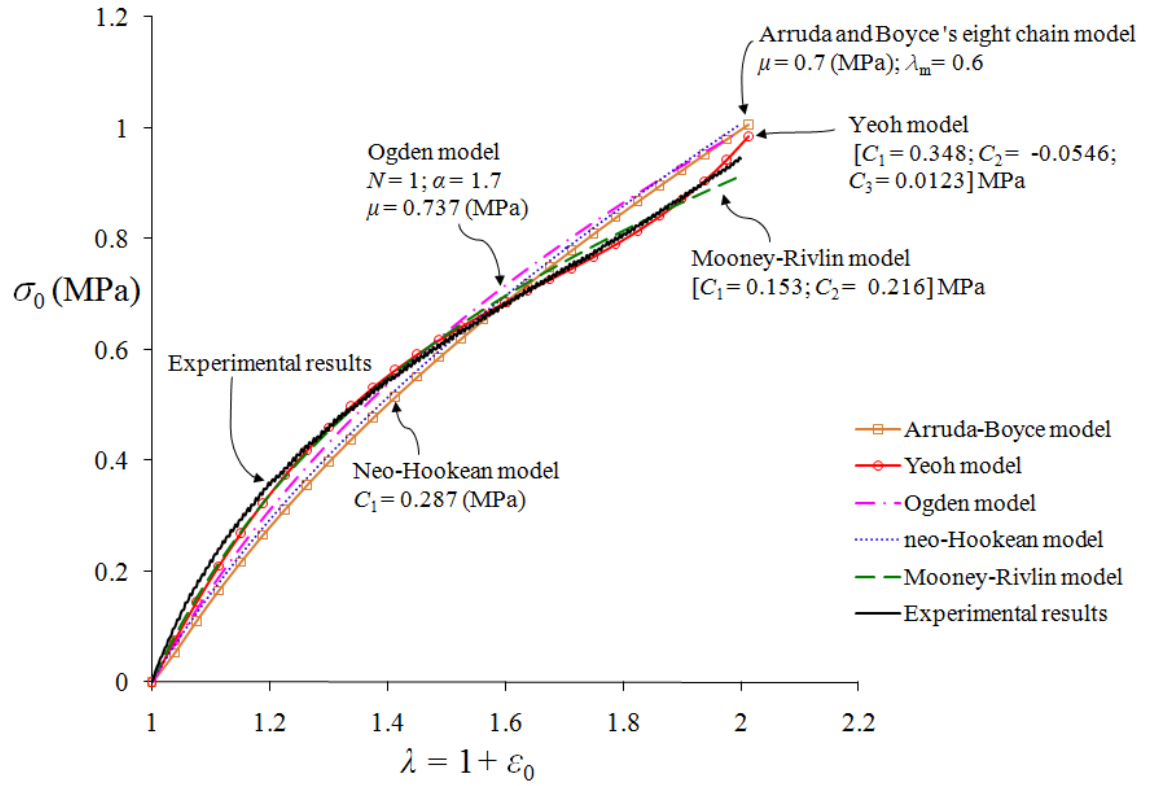
Figure 3.7 ABAQUS characterization of experimental data using different forms of strain energy function
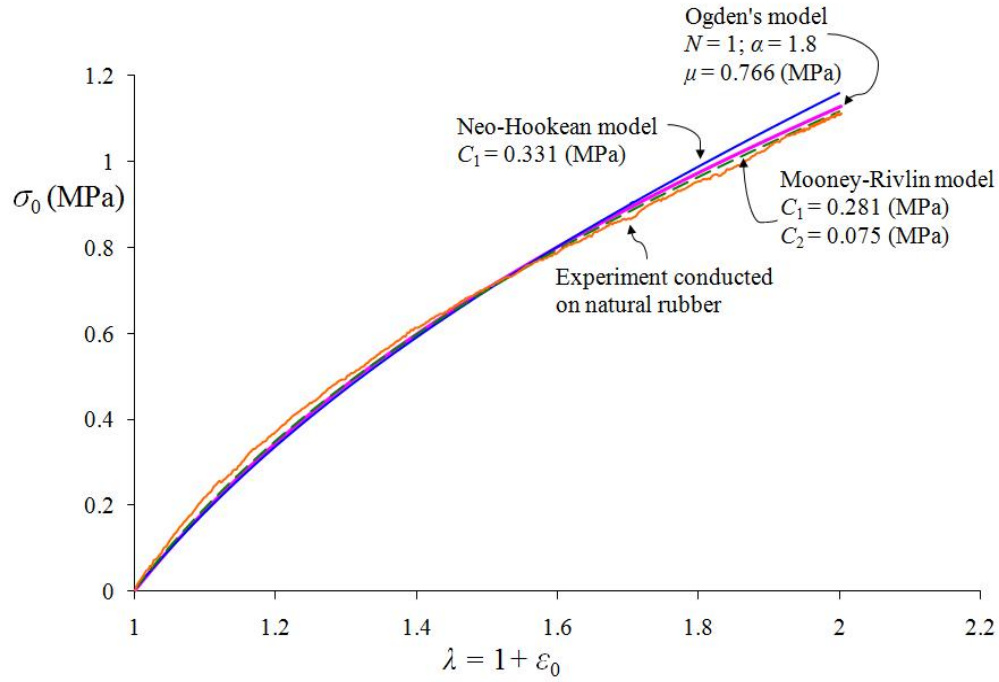
(a) Membrane thickness: 0.793 mm
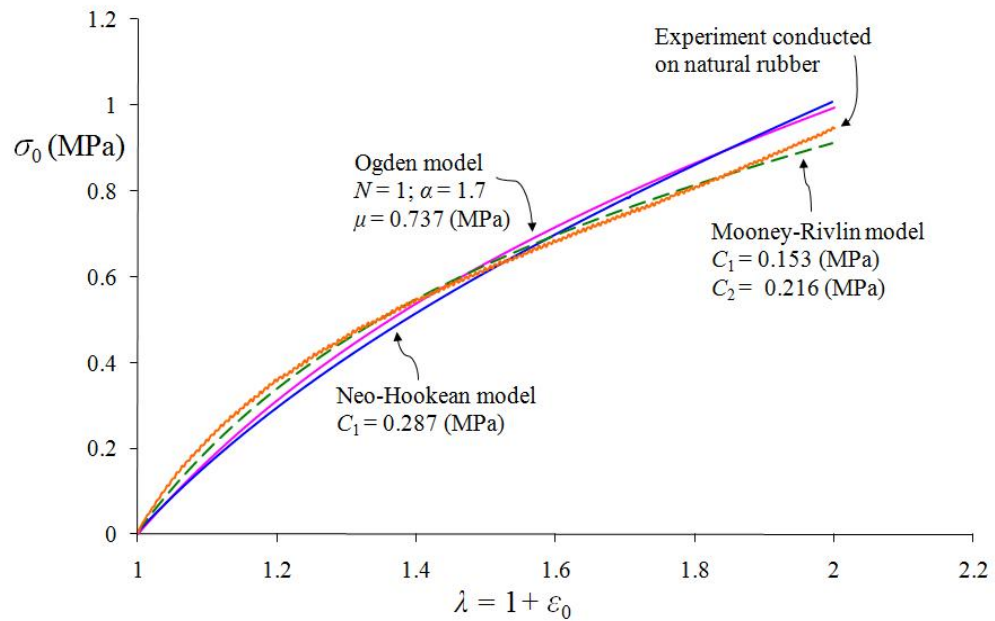
(b) Membrane thickness: 1.588 mm

Figure 3.8 Constitutive modelling of the stress-strain curve for natural rubber (corresponding to a loading rate of $\dot{\varepsilon} = 20\% / \text{min}$) using different forms of strain energy function – parameters determined from ABAQUS subroutine for material parameter identification for hyperelastic materials

3.4   The Mooney-Rivlin Parameters

The Mooney-Rivlin strain energy function is the mostly commonly used hyperelastic model that describes the mechanical behaviour of natural rubber. This model is known to give a simple representation of rubber-like solids and the simple way of determining the material parameters also makes it very convenient to use. For the case of uniaxial tension of the Mooney-Rivlin material, the stress-strain equation (2.18) can be plotted as $\sigma_0 / 2(\lambda - \lambda^{-2})$ vs. λ^{-1}, as shown in Figure 3.9.
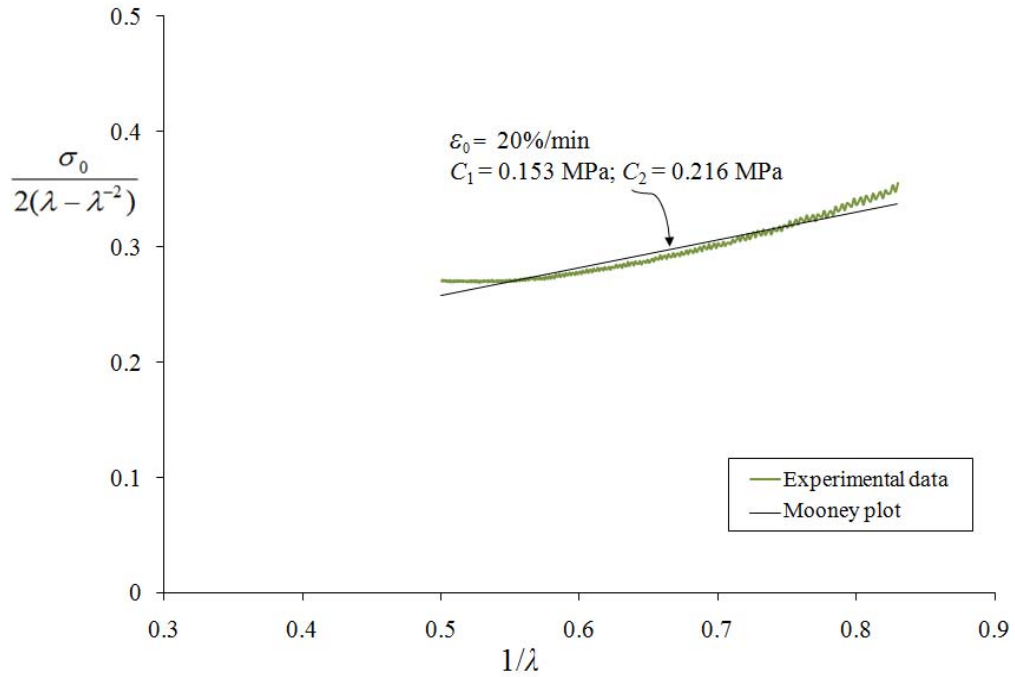
Figure 3.9   Mooney plot from uniaxial stretching of a rubber membrane with $C_1 = 0.153$MPa and $C_2 = 0.216$MPa

The above figure is referred to as a Mooney-plot with a slope of C_2 and an intercept C_1 (as $1/\lambda \rightarrow 0$). The data was obtained experimentally, during the uniaxial stretching of rubber specimens. An important observation is that a true Mooney-Rivlin material would give a straight line and not a non-linear plot, as shown in Figure 3.9. The linear fit is obtained using a least squares and regression analysis.

A number of methods can be used to determine the parameters of the Mooney-Rivlin model. Since the Mooney-Rivlin model is a generalization of the neo-Hookean model, the strain energy function is related to the Cauchy-Green stress tensor through the shear modulus, G. The linear elastic shear modulus is related to the material constants by

$$G = 2(C_1 + C_2) \tag{3.1}$$

For incompressible materials, the initial Young's modulus is given by

$$E = 6(C_1 + C_2). \tag{3.2}$$

Equation (3.2) is obtained from the relationship between the shear modulus and the modulus of elasticity for isotropic linear elastic materials,

$$G = \frac{E}{2(1+v)}. \tag{3.3}$$

For incompressible materials, $v \approx 0.5$ and

$$3G = E. \tag{3.4}$$

Table 3.1 presents the Mooney-Rivlin constants obtained in section 3.3 and their respective shear moduli. The values of G for each thickness should theoretically be the same since both samples are from the same type of rubber. It was found from the uniaxial test results that the Mooney-Rivlin constants can vary; a small range of Mooney-Rivlin constants can exist for the material, as long as equation (3.1) is satisfied (Figure 3.10).

Table 3.1   The Mooney-Rivlin constants and the shear moduli

Specimen thickness (mm)	C_1 (MPa)	C_2 (MPa)	G (MPa)
0.793	0.281 ± 0.02	0.075 ± 0.02	0.712 ± 0.04
1.588	0.153 ± 0.02	0.216 ± 0.02	0.738 ± 0.04
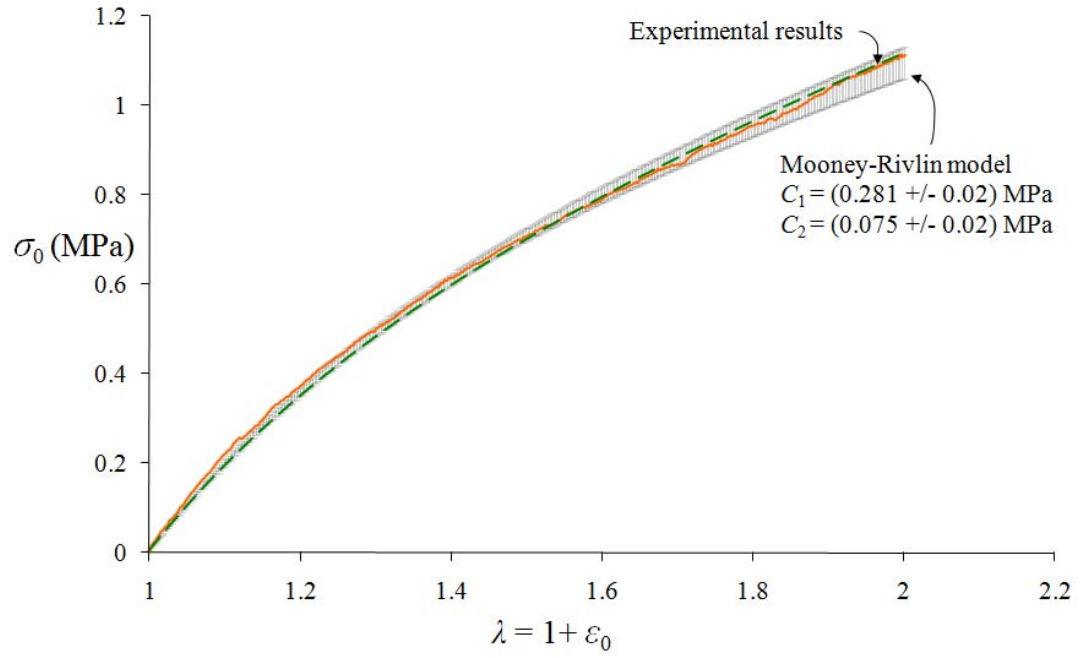
(a) Membrane thickness: 0.793 mm
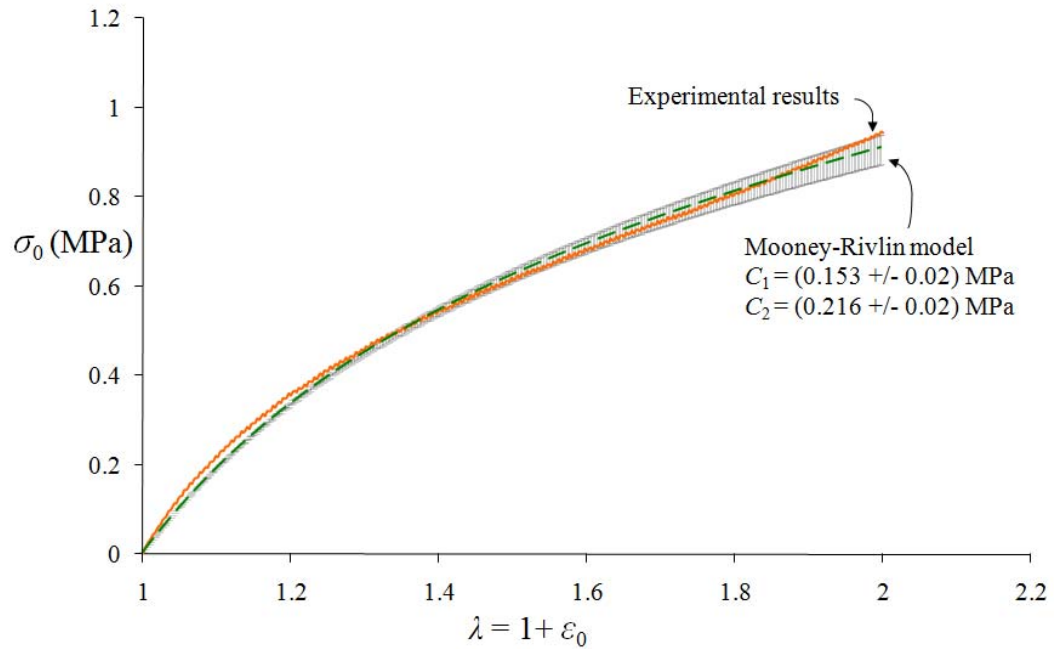
(b) Membrane thickness: 1.588 mm

Figure 3.10   Range for the Mooney-Rivlin constants

Chapter 4

FLUID LOADING OF A RUBBER MEMBRANE

4.1 Introduction

To validate the results of the constitutive model development, a further experiment was conducted, where the rubber membrane was subjected to a multi-axial state of stress. The specific problem chosen for the experimental study is that of a natural rubber membrane that was fixed along a circular boundary and subjected to a fluid load applied in the transverse direction (Figure 4.1). The membrane loading was selected to induce strains in the same range as those applied to determine the constitutive properties of the rubber.
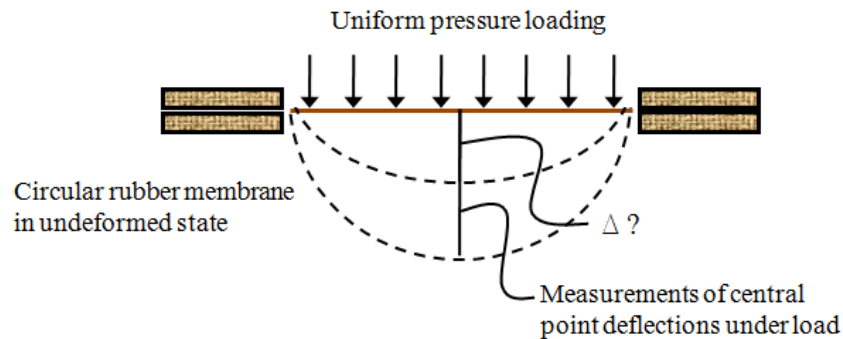
Figure 4.1 Two-dimensional schematic view of the experiment

4.2 The Test Facility

Photographic and schematic views of the experimental facility used to conduct fluid loading of the rubber membrane are shown in Figures 4.2 and 4.3, respectively. The apparatus consists of a series of precision manufactured glass cylinders of internal diameter 15 cm, length 61 cm and wall thickness of 0.50 cm that are connected to form a unidirectional column of height 260 cm. This test facility was used by Dong (2006) and

Selvadurai and Dong (2006) in their studies dealing with advective transport of chemicals in porous media. Smooth walled glass cylinders were used to provide a relatively distortion-free transparent surface for the observation of the fluid and to minimize any damage to the interior surface in cases where solid material might be added in subsequent experiments. The fluid used in this experiment was tap water at approximately 24$^{\mathrm{o}}$C. The membrane testing set-up was adapted to apply fluid loading to a membrane that was fixed along a circular boundary. The rubber membranes used were 146 mm in diameter with thicknesses of 0.794 mm and 1.588 mm. A total of three experiments were performed for each thickness. The fixed boundary condition was achieved by clamping the membrane between a plexiglass and an aluminum plate. The boundaries of the plexiglass and aluminum plates were shaped to a circular cross section to minimize stress concentration along the clamped edge. Careful placement of the membrane was necessary to prevent both leakage and slippage. To prevent leakage between the glass column and the membrane, two rubber gaskets sandwiched the membrane and a thin aluminum plate was placed at the bottom; the membrane-plate assembly was secured with 8-32 screws. The schematic view of the clamped assembly is shown in Figure 4.4a. Previous tests on a rubber membrane indicated that slippage occurred at the fixed end (Selvadurai and Yu (2006)). To eliminate this effect, an additional layer of hard neoprene rubber was bonded on one side of the membrane, using a non-reactive adhesive – Lepage ® Pres-Tite Green contact cement (Figure 4.4b and c). Observations indicated that this additional layer eliminated the slippage problem and prevented tearing of the rubber membrane at the clamping edge. Furthermore, since the preparation and experiment duration are relatively short (less than an hour), the possibility of any long-term chemical reaction between the adhesive and the rubber membrane were neglected.
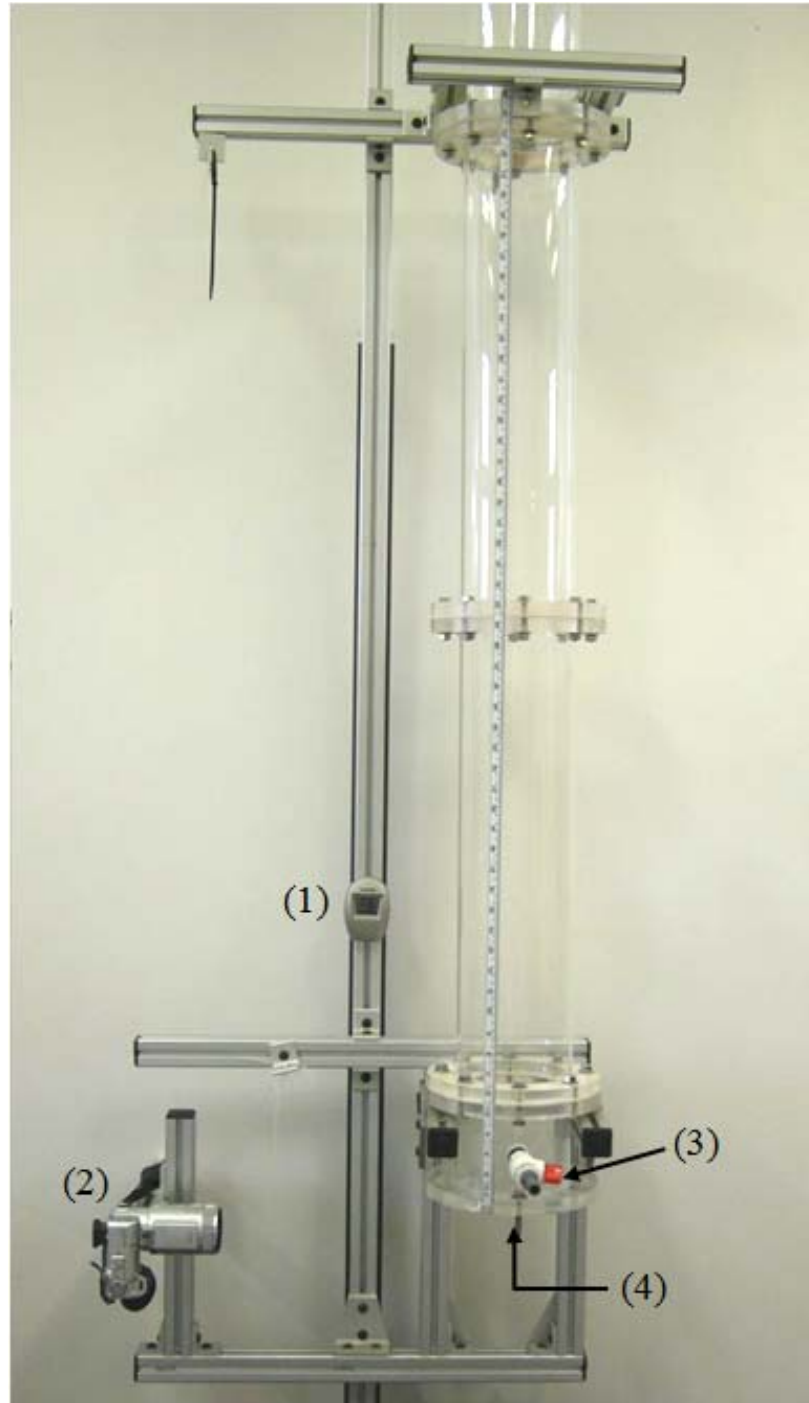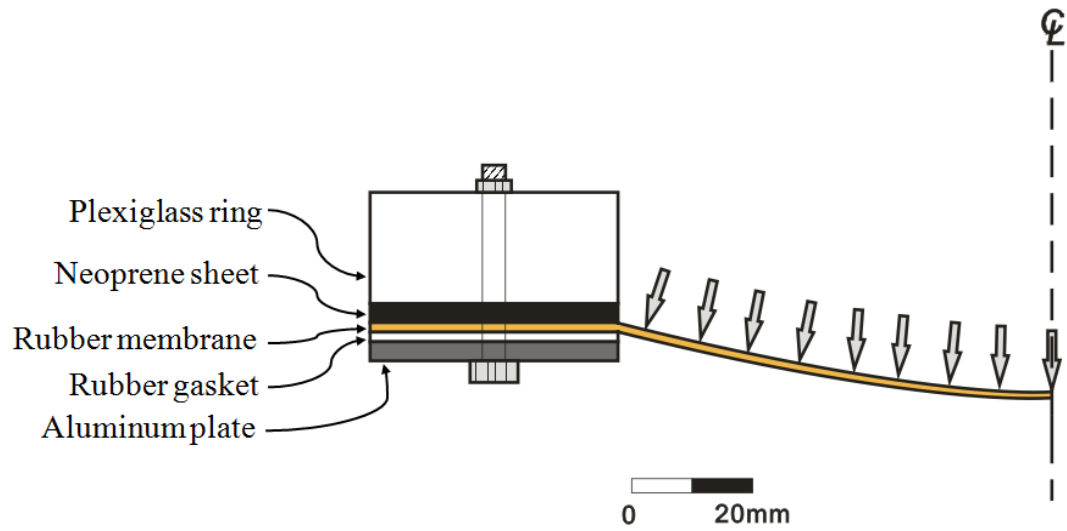
(1) Digital thermometer; (2) Digital camera;
(3) Inlet/Outlet Valve; (4) Rubber membrane

Figure 4.2 Photographic view of the experimental apparatus
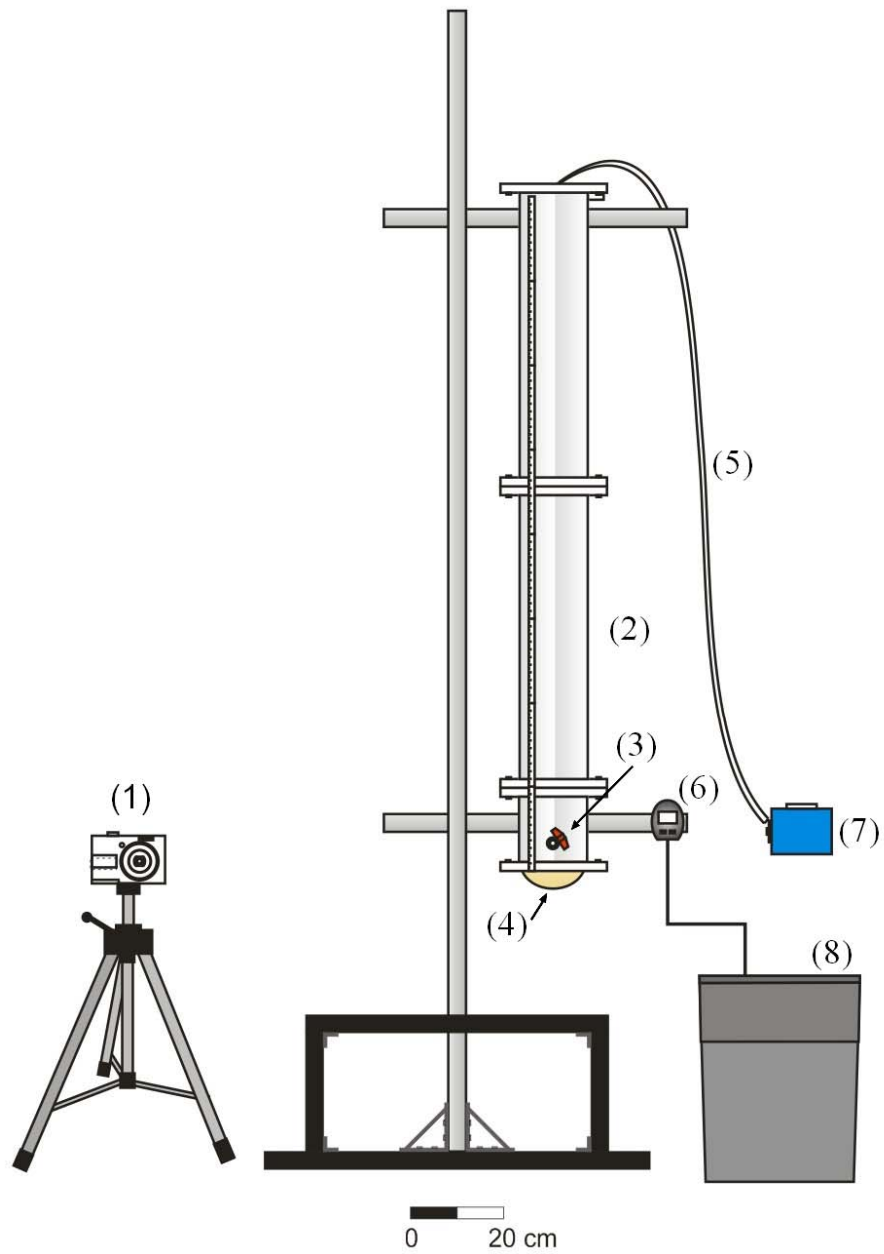
(1) Digital camera; (2) Fluid columns; (3) Inlet/outlet valve; (4) Rubber membrane;
(5) Plastic tube; (6) Digital thermometer; (7) Pump; (8) Water container

Figure 4.3   Schematic view of the experimental apparatus

(a) Schematic view of the clamped assembly

Plexiglass ring
Neoprene sheet
Rubber membrane
Rubber gasket
Aluminum plate

0   20mm

(b) Lepage Pres-Tite Green contact cement

Dia. = 146 mm
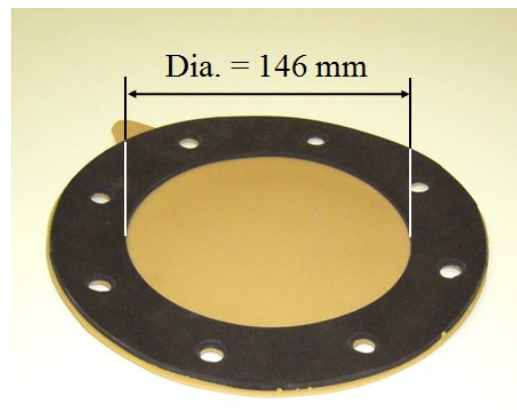
(c) Rubber membrane specimen with hard neoprene restraint

**Figure 4.4**   Details of the rubber membrane

4.3   Experimental Results

The measurement of the deflected shape of the rubber membrane for different pressures was the main focus of this experimental research, and results would then be validated using a finite element simulation. The deflected profile was examined by applying a fluid load in an incremental manner until the rubber membrane reached a strain of approximately 100%. The deflected profile was measured using an optical technique; using a high precision (5 Mega pixels) digital camera, a photographic record of the deflected profile was captured for each successive pressure increment. The distance of the camera to the test specimen does not require a fixed location since the data extraction procedure of the visual images is related to a distance in image *pixels* rather than the actual physical distance. However, the central optical axis of the camera must be aligned and normal to the datum of the object. In the experiments, the datum was taken as the midpoint of the rubber membrane in its median plane. The camera was positioned to capture a representative focused image through the plane of symmetry of the membrane. To obtain the deformation at the central deflection, the image *pixels* are calibrated against a known physical distance, which in this case is the diameter of the aluminum plate. The physical deflection of the membrane can then be determined by converting between the image pixels and the known distance. This method was found to minimize any parallax or barrel distortion. The image resolution is an important factor for the accuracy of the data. An image resolution of 2304 x 1728 pixels was used and proved to give accurate results. During the experiment, the images of the deflected profile were recorded for different water heights. A total of three experiments were performed for each rubber thickness. Water was added to the column in an incremental manner of 10 cm up to a central maximum displacements of $\Delta_{max} = 63.9$ mm and $\Delta_{max} = 51.5$ mm for the 0.793 mm and 1.588 mm thick rubber membranes, respectively. The load-displacement response is shown in Figure 4.5. The strain in the membrane at different pressures was measured using the same optical technique described earlier. A uniform grid was drawn on the rubber membrane using a fine black marker with spacings of 10 mm between gridlines. As the membrane stretched, the gridlines were used to calculate the strain at different pressures. It was found that the central maximum displacement corresponds

approximately to an overall average strain of 113% and 70% in the radial direction for the 0.793 mm and 1.588 mm thick rubber membranes, respectively. The load-strain results are shown in Figure 4.6. The results show a good repeatability between sets of experiments.
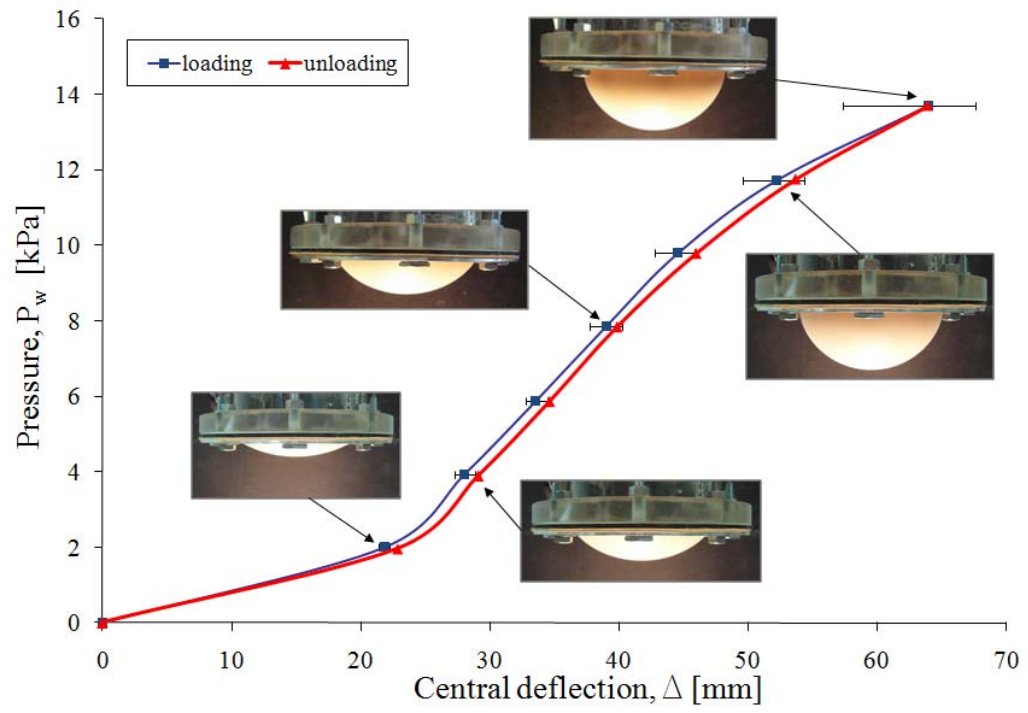
(a) Membrane thickness: 0.793 mm
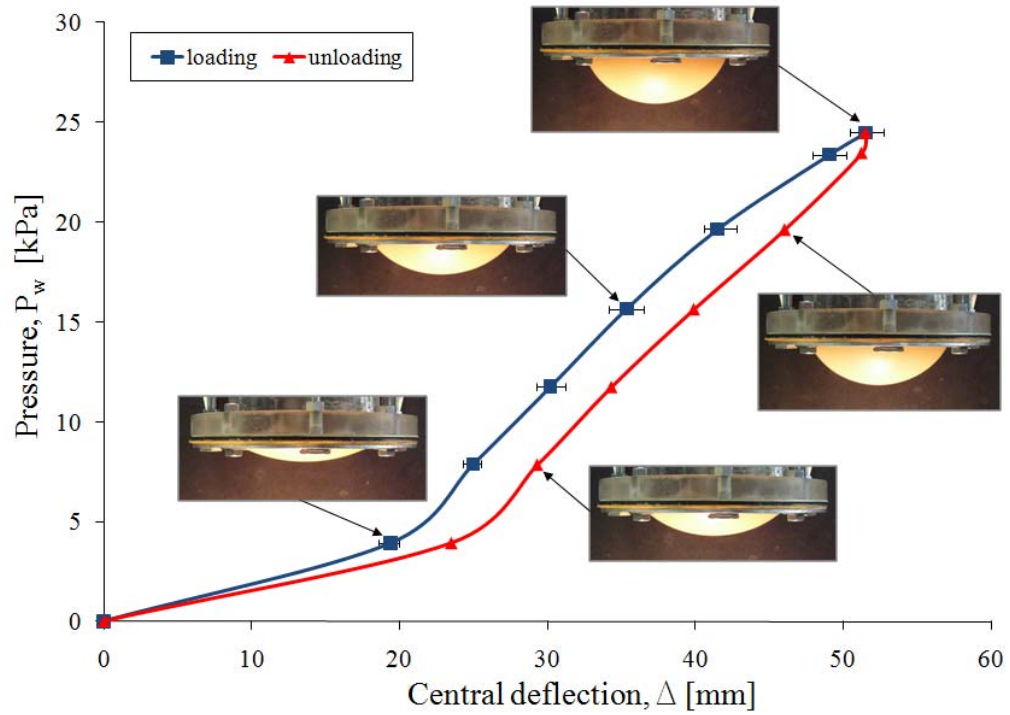
(b) Membrane thickness: 1.588 mm

Figure 4.5 Load-displacement responses for the fluid loading experiment
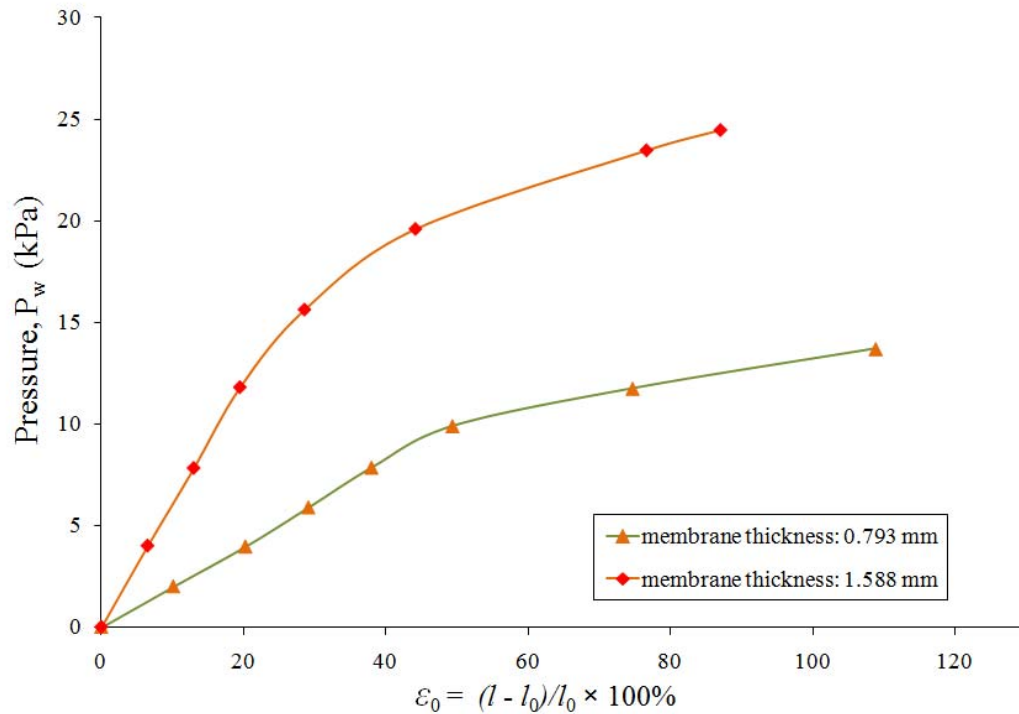
Figure 4.6   Load-strain results for the fluid loading experiment

4.4   Technical Specifications of Experiment Facility

This section presents the technical specifications of the materials and components used in the experiments. This information is provided for completeness and for future use.

Natural gum rubber sheets

- Thicknesses: 1/32 in (0.793 mm) and 1/16 in (1.588 mm)
- Durometer 35 ShoreA
- Temperature range: $-20\,^{\circ}\text{F}$ to $140\,^{\circ}\text{F}$ ($-28\,^{\circ}\text{C}$ to $60\,^{\circ}\text{C}$)
- No oil resistance
- Excellent acid resistance
- Supplier: Murdock Industrial, Akron, USA

Neoprene sheets (black)

- Thickness: 1/8 in (3.175 mm)
- Durometer 70 ShoreA
- Temperature range: -40°F to 275 ^{o}F (-40 ^{o}C to 135°C)
- Good oil resistance
- Good ethanol resistance
- Low acetone and chlorine resistance
- Supplier: Johnston Industrial Plastics, Montreal, Canada

MLP-500 Load cell

- Sensor model: MLP-500
- Serial number: 221356
- Capacity range: 500 lbs (2224 N)
- Accuracy: +/- 0.5 lbs (2.2 N)
- Excitation: 10 VDC
- Supplier: Transducer Techniques, Temecula, USA

Glass tubes

- Internal diameter: 15 cm
- Outside diameter: 15.5cm
- Simax heat resistant
- Supplier: Kavalier, Sazava, Czech Republic

Glass thermometer

- Indoor and outdoor temperature reading
- Temperature range: -35°C to 50°C
- Accuracy: +/-1°C
- Supplier: McMaster-Carr, Aurora, USA

Digital camera: Panasonic Lumix DMC-Z2

Lepage ® Pres-Tite Green contact cement

- Strong bond with plywood, metal, rubber, etc.

- Excellent creep resistance

- Purchased at RONA, Montreal, Canada

Instant Krazy Glue ® pen

- Strong bond with wood, rubber, glass, metal, plastic and ceramic

- Purchased at Canadian Tire, Montreal, Canada

Plastic tubing

- Outside diameter: 1/2 in (12.7 mm)

- Thickness: 3/8 in (9.5 mm)

- Length: 20 feet (6.1 m)

- Purchased at RONA, Montreal, Canada

Submersible pump

- Model: 4E-34NR

- Horsepower 1/12

- Flow 810 GPH (1066 LPH) at 1 ft of head

- 210 Watts

- Thermal overload protection

- Supplier: Little Giant Pump Company, Oklahoma City, USA

Chapter 5

COMPUTATIONAL MODELLING OF FLUID LOADING OF RUBBER MEMBRANE

5.1 Introduction

This chapter describes the finite element modelling of the hyperelastic behaviour of the natural rubber membrane subjected to fluid pressure. The modelling used the commercial finite element software ABAQUS (ABAQUS/Standard (2008)). This code contains many features related to the modelling of large strain phenomena, including the possibility of implementing a chosen constitutive model into the computational algorithm. This program is used extensively for the study of problems related to hyperelastic materials. The objective here is to model a rubber membrane that is subjected to different pressures, observe its central deflection and to compare the computational predictions with experimental observations. The Mooney-Rivlin constitutive model with the material parameters determined in Chapter 3 is used in the computational modelling.

5.2 Rubber Membrane Model

The circular rubber membrane was modelled as a three-dimensional structure. Since the thickness of the specimen is small compared to its radius and since the fluid pressure loading transforms the flat membrane into a curved thin shell, a three-dimensional deformable shell element was used to create the model. Although a two-dimensional model would also be applicable for this case, due to the symmetry of the structure, a three-dimensional model gives a better overall visual representation of the deformed shape at different pressures. Also, since both the two-dimensional and the three-dimensional models gave the same results for the deflected shape and since the mesh

generation and computing time had little effect on the overall analysis, the three-dimensional option was chosen.

5.3   Membrane Elements

Membrane elements were chosen to model the circular rubber membrane. The use of membrane elements is appropriate for non-linear analyses; these elements represent thin surfaces that transmit forces in its plane but have no bending stiffness.   ABAQUS offers a number of membrane elements in its element library, each of which is placed in three different categories: general membrane elements (M3D3, M3D4, M3D4R, M3D6, M3D8, M3D8R, M3D9, M3D9R), which include both triangular and quadrilateral types of elements, cylindrical membrane elements (MCL6, MCL9) and axisymmetric membrane elements (MAX1, MAX2, MGAX1, MGAX2).   General membrane elements are used in most three-dimensional models in which the deformation of the structure can evolve in three dimensions. Cylindrical membrane elements should be chosen for precise modeling of regions in a structure with circular geometry, such as tires. It is useful when displacements along the circumferential direction need to be determined. Axisymmetric membrane elements allow torsion loading and general material anisotropy.   The membrane model used in this research consists of M3D8R elements – quadrilateral, 8 noded with reduced integration (Figure 5.1). Each node has three displacement and three rotation degrees of freedom. The choice of specific element type is explained below.
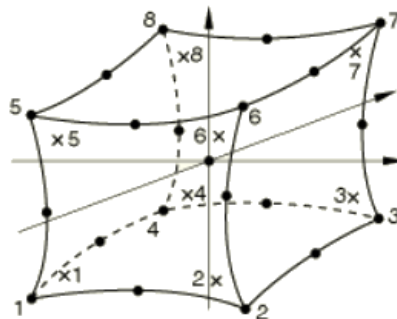

Figure 5.1   Quadrilateral 8-node reduced integration element
(ABAQUS, 2008)

Either triangular or quadrilateral elements could be used for the analysis of the membrane. The choice depends upon the complexity of the structure, the mesh geometry, the size aspect ratio, the accuracy of the results required as well as minimizing computing time. Since the membrane structure has a very simple geometry, it was found that the computing time was the same regardless of the choice of the element. Therefore, quadrilateral elements were chosen over triangular elements since they have a better convergence rate and no sensitivity to mesh orientation.

The second-order form of the quadrilateral elements was selected because it provides higher accuracy for problems that do not involve complex contact conditions or severe element distortions in the analysis. Second order elements have extra mid-side nodes in each element making computation of small and finite deformations more effective.

The reduced-integration option is preferred for quadratic elements because it uses a lower-order integration to produce the element stiffness and decreases the computing time of an analysis, especially in three dimensions. Also, since the accuracy of the analysis is of prime importance, second-order reduced integration elements were chosen because this typically yields more accurate results than the first order elements.

5.4   Alternative: Solid Elements

Solid (continuum) elements could have also been used to model the rubber membrane. Numerical simulations indicated a less than 0.3% difference in the results for the maximum deflection of the rubber membrane if either the solid or membrane element type was chosen. Solid elements have a hybrid incompressible formulation (ABAQUS/Standard (2008)) since they are intended primarily for use with incompressible and almost incompressible materials. For nearly incompressible cases (where the Poisson's ratio, ν, is greater than 0.4999999), the material will produce extremely large changes in pressure for a very small change in displacement. Hybrid elements treat the isotropic pressure p as an independently interpolated basic solution
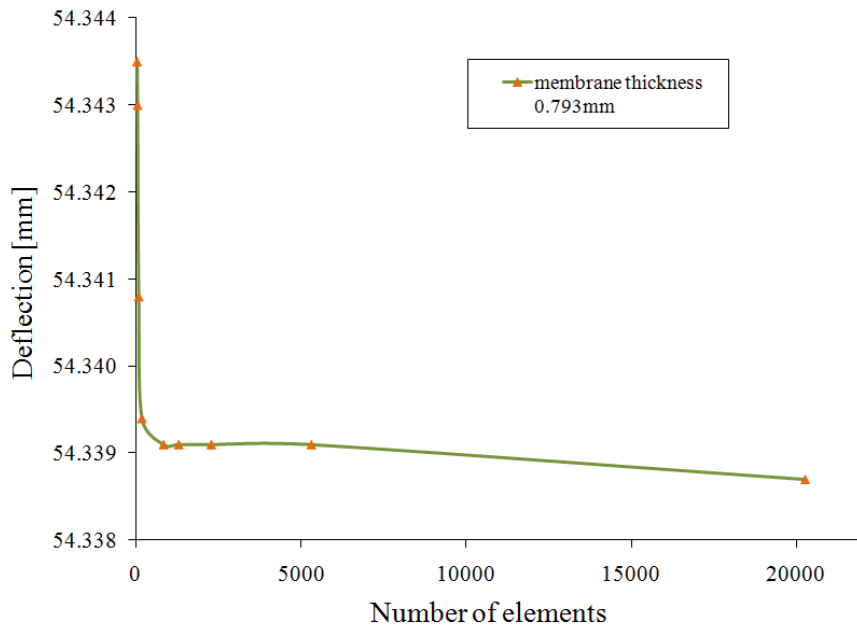
variable and couple it to the displacement. ABAQUS recommends the use of hybrid solid elements for hyperelastic materials.
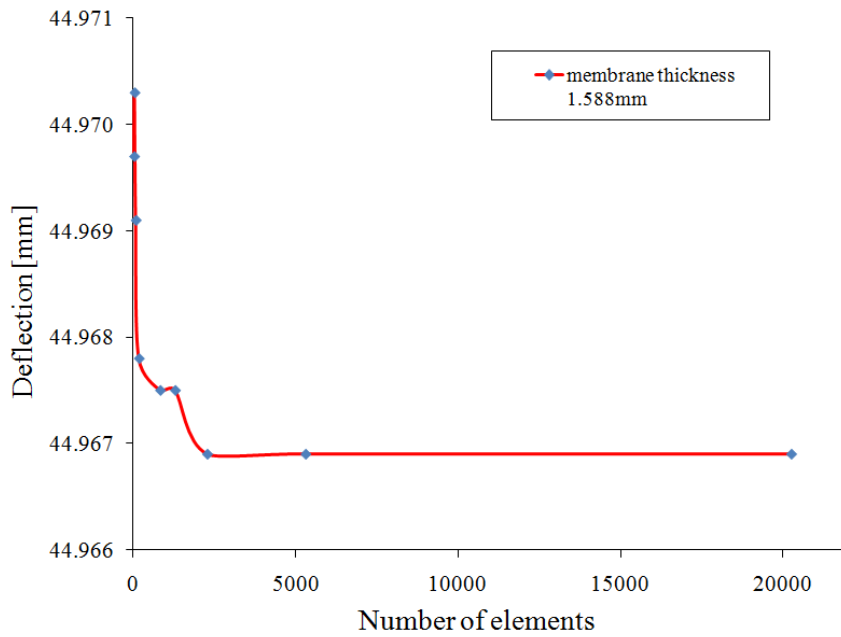
5.5 A Convergence Study

A convergence study was conducted to determine if the uniform mesh size of the final model provided accurate results and whether or not there should be a mesh refinement or coarser meshes should be used to reduce the computing time during analysis. The maximum deflection at the central point of the membrane was computed for different mesh sizes. The number of elements used for the membrane ranged from 42 to 20, 266. The results of the convergence study are presented numerically in Table 5.1 and graphically in Figure 5.2. Based upon the results, the model which consisted of 840 and 2, 287 elements for the membranes of thickness 0.793mm and 1.588mm, respectively, provided satisfactory accuracy.

Table 5.1 Results of a convergence study

(a) Membrane thickness: 0.793mm

Number of membrane elements	Maximum central deflection (mm)
42	54.3435
56	54.3430
92	54.3408
188	54.3394
840	54.3391
1300	54.3391
2287	54.3391
5315	54.3391
20266	54.3387

(b) Membrane thickness: 1.588mm

Number of membrane elements	Maximum central deflection (mm)
42	44.9697
56	44.9703
92	44.9691
188	44.9678
840	44.9675
1300	44.9675
2287	44.9669
5315	44.9669
20266	44.9669

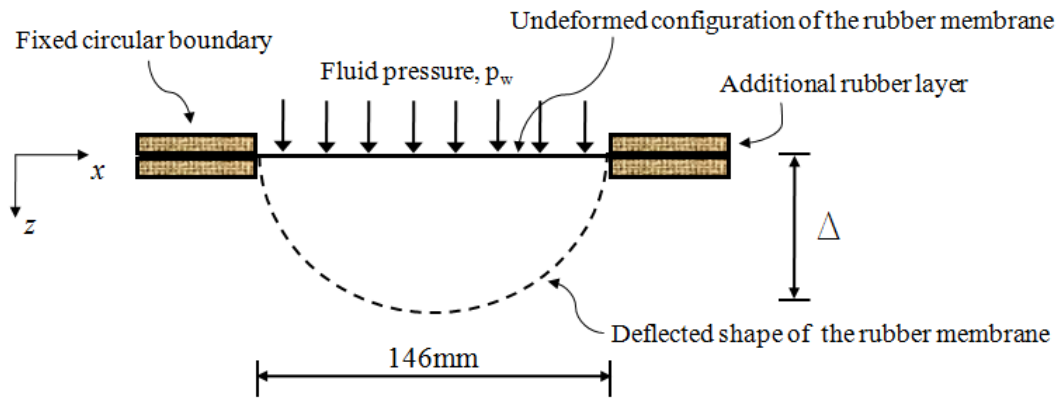(a) Membrane thickness: 0.793mm

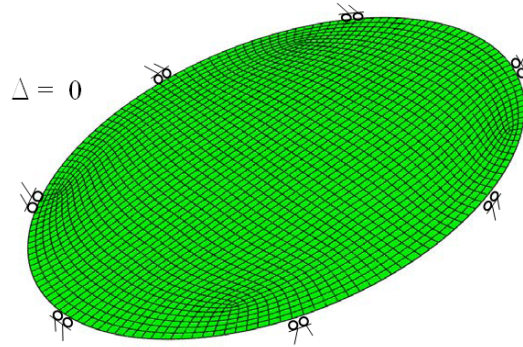(b) Membrane thickness: 1.588mm

Figure 5.2　Convergence analysis
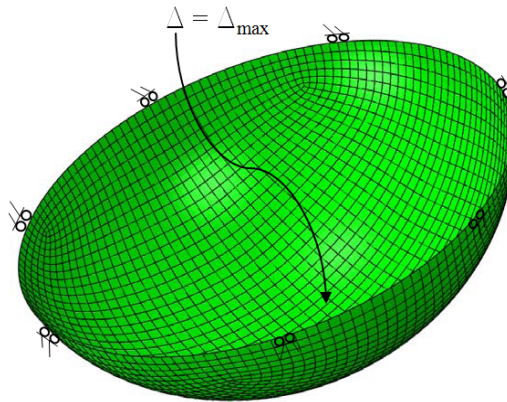
5.6   Computational Results

The schematic view of the rubber membrane problem under fluid loading is illustrated in Figure 5.3a.   The boundary conditions and finite element discretization used in the computational modelling are shown in Figure 5.3b.   The boundary condition of the membrane is fixed; i.e., neither a displacement nor a rotation is allowed.   Uniform pressure is applied on the membrane surface for pressures up to 13.7 kPa and 24.5 kPa for the membranes of thickness 0.793 mm and 1.588 mm, respectively.   The Mooney-Rivlin material model is used for the rubber with the constants obtained from uniaxial tests: $C_1 = 0.281$ MPa and $C_2 = 0.075$ MPa for the thinnest membrane, and $C_1 = 0.153$ MPa and $C_2 = 0.216$ MPa for the thicker membrane.   A constant pressure was assumed to act on the membrane (Figure 5.4).   It was found that the influence of the weight of the fluid in the deformed region can be neglected; the difference between the real and the assumed pressure corresponds to a discrepancy of approximately 2%, which falls within the range of accuracy of the tests.   Figure 5.5 and Table 5.2 show the comparison of the load-displacement responses between the computational predictions and the experimental results.   It can be seen that the computations are accurate for pressures below 12 kPa and 22 kPa for the membranes of thickness 0.793 mm and 1.588 mm, respectively, but they under estimate the experimental results for higher pressures.   For purposes of comparison, Table 5.2 also presents the results for the unloading mode.   One can see that due to the presence of nominal hysteresis in the real membranes, the error between the computational and experimental results is increased for the unloading portion.   Overall, the computational results provide a comparable trend and a satisfactory prediction of the deflection of the membrane determined from the experiments.

(a) Fluid loading on rubber membrane

(b) Mesh configuration and boundary conditions
(total number of elements: 840 and 2287, for membranes of thickness
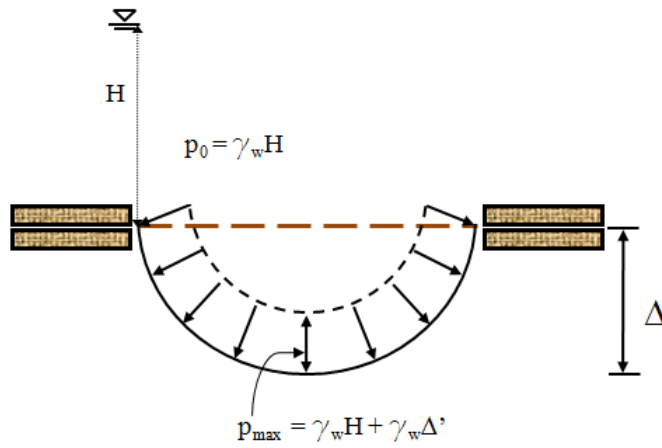0.793 mm and 1.588 mm, respectively)

(c) Deformed shape under maximum loading
(Δ_{max} = 63.9 mm and Δ_{max} = 51.5 mm for the 0.793 mm and 1.588 mm
thick rubber membranes, respectively)

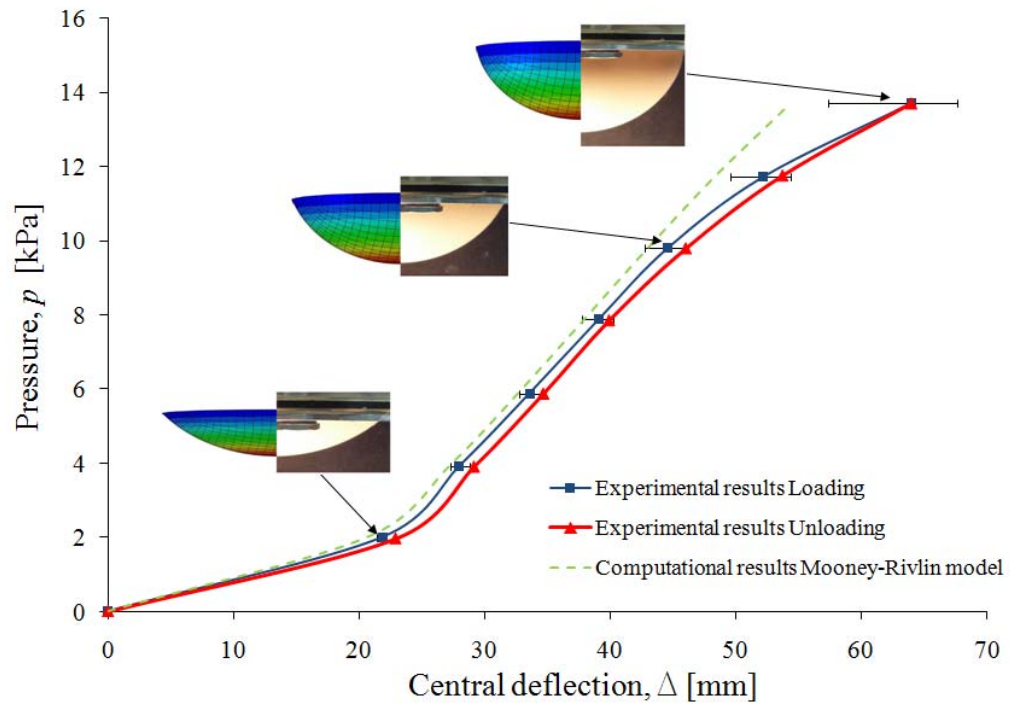**Figure 5.3** Computational results for the deflection of the rubber membrane

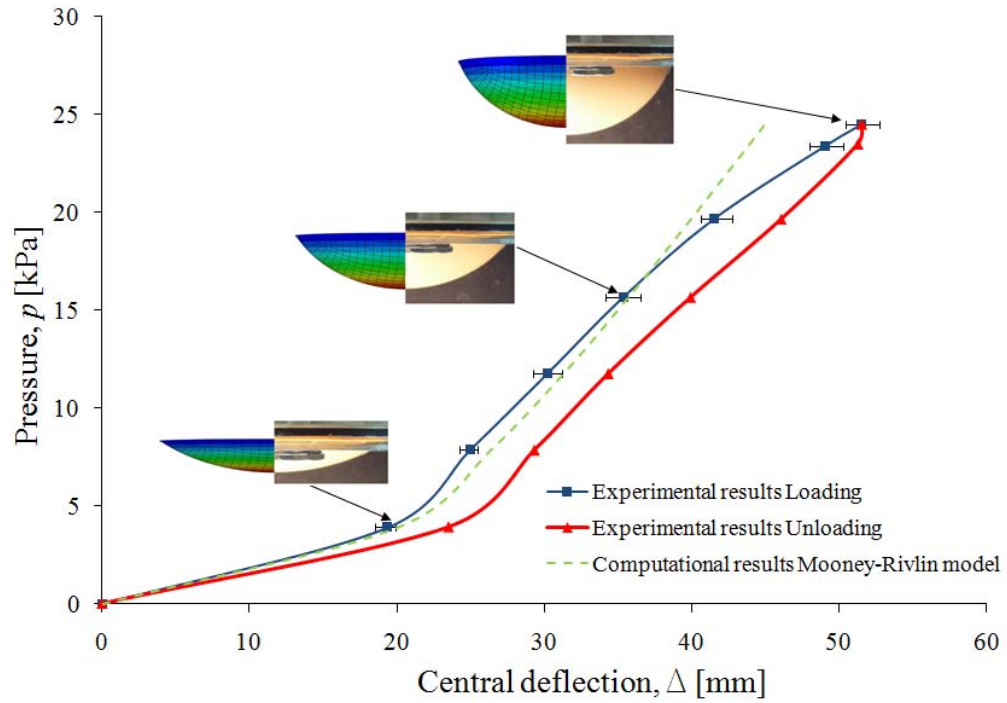47
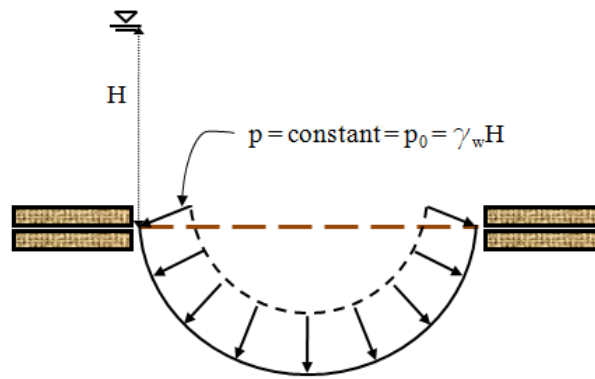
(a) Assumed uniform pressure

(b) Real (non-uniform) pressure

Figure 5.4 Pressure of the fluid on the deformed membrane
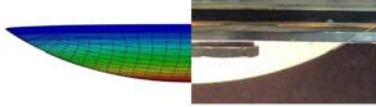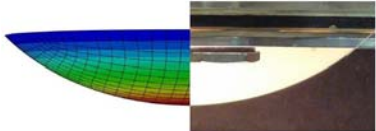
(a) Membrane thickness: 0.793mm

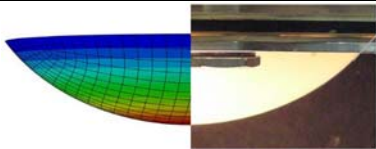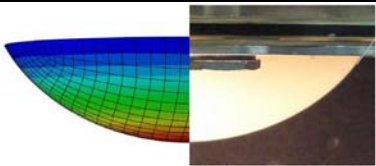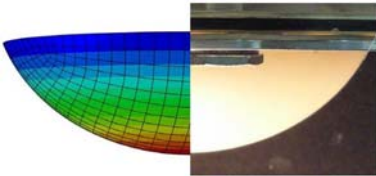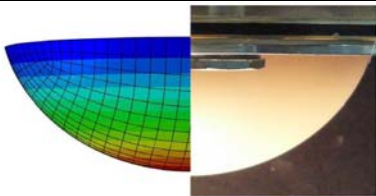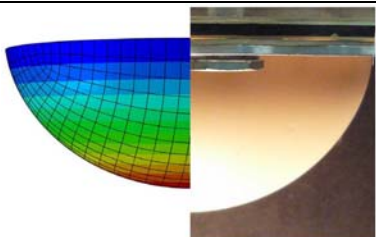(b) Membrane thickness: 1.588mm

Figure 5.5   Comparison of experimental results and computational predictions

Table 5.2 Experimental and computational comparison of load-displacement responses of the thin rubber membrane

(a) Membrane thickness: 0.793 mm;

  Mooney Constants: $C_1 = 0.281$ MPa ; $C_2 = 0.0075$ MPa

Experimental vs. Computational deflected profile	Pressure (kPa)	$\%\,Error = \dfrac{\Delta_{max}^{Exp} - \Delta_{max}^{Comp}}{\Delta_{max}^{Exp}} \times 100\%$
LOADING		
	2.0	5.3
	3.9	2.8
	5.9	2.7
	7.9	2.9
	9.8	3.5
	11.7	7.4
	13.7	15.0

(b) Membrane thickness: 0.793 mm;
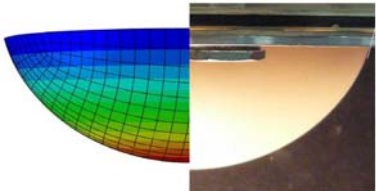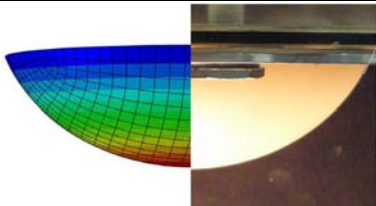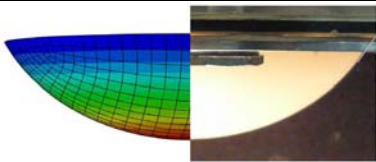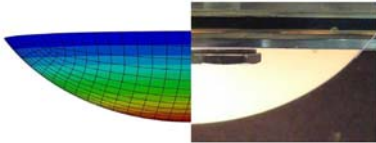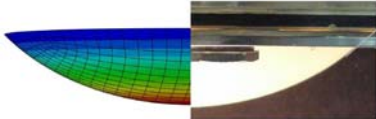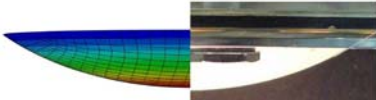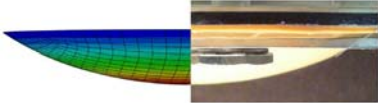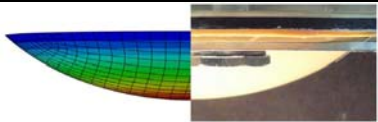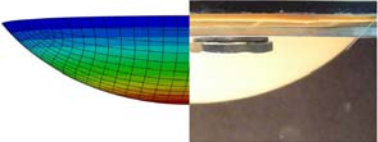
Mooney Constants: $C_1 = 0.281$ MPa ; $C_2 = 0.0075$ MPa

Experimental vs. Computational deflected profile	Pressure (kPa)	$\%\,Error = \dfrac{\Delta_{max}^{Exp} - \Delta_{max}^{Comp}}{\Delta_{max}^{Exp}} \times 100\%$
UNLOADING		
	11.8	10.0
	9.8	6.5
	7.8	4.9
	5.9	5.7
	3.9	6.6
	2.0	7.6

51

Table 5.3   Experimental and computational comparison of load-displacement responses of the thick rubber membrane
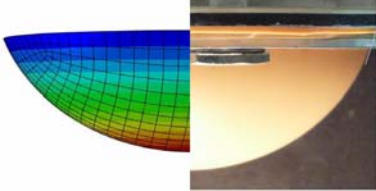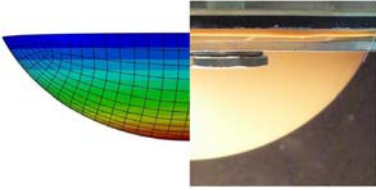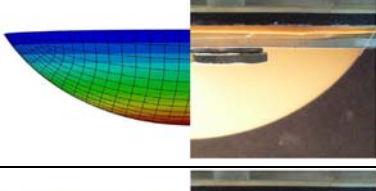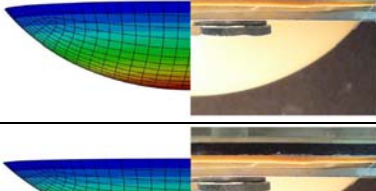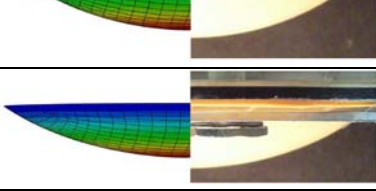
(a) Membrane thickness: 1.588mm;

Mooney Constants: $C_1 = 0.153$MPa ; $C_2 = 0.216$MPa

Experimental vs. Computational deflected profile	Pressure (kPa)	$\%\,Error = \dfrac{\Delta_{max}^{Exp} - \Delta_{max}^{Comp}}{\Delta_{max}^{Exp}} \times 100\%$
LOADING		
	3.9	3.5
	7.8	5.5
	11.7	3.7
	15.6	1.1
	19.7	3.7
	23.4	10.6
	24.5	12.7

(b) Membrane thickness: 1.588mm;

Mooney Constants: $C_1 = 0.153$MPa ; $C_2 = 0.216$MPa

Experimental vs. Computational deflected profile	Pressure (kPa)	$\%\,Error = \dfrac{\Delta_{max}^{Exp} - \Delta_{max}^{Comp}}{\Delta_{max}^{Exp}} \times 100\%$
UNLOADING		
	23.5	14.4
	19.6	13.2
	15.6	10.5
	11.7	8.8
	7.8	10.0
	3.9	14.7

Chapter 6

CONCLUSIONS AND RECOMMENDATIONS FOR FUTURE WORK

6.1   Summary and Conclusions

In this thesis, the mechanical behaviour of natural gum rubber membranes of two different thicknesses was studied. Several hyperelastic models have been developed to describe the behaviour of rubber for a large range of strains. The objective of this work w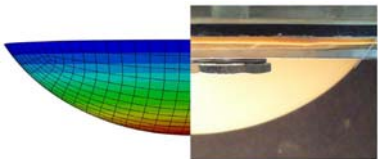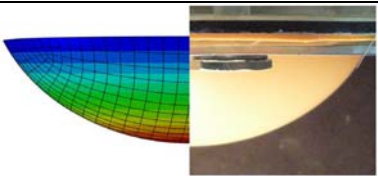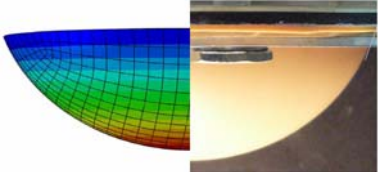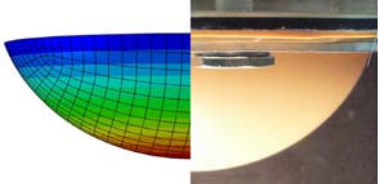as to choose the simplest model that can provide the best match for the stress-strain data obtained from uniaxial tensile tests and validate the material parameters through membrane load tests and computational modelling.

The membrane loading test can be regarded as a useful testing method for investigating hyperelastic rubber-like materials. The application of fluid loading allows control over the deformation behaviour and the optical technique allows accurate measurement of the deflected profile at different pressures. The experimental and computational results showed that the degree of correlation is consistent with that observed in the range of strains applicable to the model development. The experimental results indicate that the Mooney-Rivlin form the strain energy function can adequately model the mechanical behaviour of the membrane at moderately-large strains (i.e. $\varepsilon_0 < 65\%$). The computational simulations indicate that the Mooney-Rivlin form of the strain energy function can adequately predict the experimental response of membranes that experience strains of up to 65% during fluid loading.

6.2 Recommendations for Future Work

One natural extension of the current work would be to study the mechanical behaviour of natural rubber at higher strain levels. It will be interesting to identify the strain energy functions associated with the new strain range and see which model provides a better match with the stress-strain experimental data.

The validation of the model parameters can be done via pressurization or indentation experiments.

One can also conduct fluid loading on natural rubber using a mixture of pure water and ballotini and observe the presence of any irreversible behaviour in the material after a certain period of time.

Another area of interest would be to study the alteration in the mechanical behaviour of a natural rubber subjected to heat, oil, oxidation or ozone. The long-term impact on the deformability, or embrittlement, and other physical and chemical transformations of the material can be interesting to analyze.

A potential lead for future work also includes the observation of the molecular structure of the rubber for different cross-linking densities, chain lengths and initial pressures or stretches.

REFERENCES

ABAQUS/Standard (2008), *A General-Purpose Finite Element Program*, Pawtucket, RI, USA.

Adkins, J.E. and Rivlin, R.S. (1952), Large elastic deformations of isotropic materials. IX. The deformation of thin shells, *Philosophical Transactions of the Royal Society of London. Series A, Mathematical and Physical Sciences*. **244** 505-531.

Alexander, H. (1971), The tensile instability of an inflated cylindrical membrane as affected by an axial load, *International Journal of Mechanical Sciences*. **13** 87-95.

Arruda, E.M. and Boyce, M.C. (1993), A three-dimensional constitutive model for the large stretch behavior of rubber elastic materials, *Journal of the Mechanics and Physics of Solids*. **41** 389-412.

ASTM (American Society for Testing and Materials) (2006), Annual Book of ASTM Standards, Vol. 9.01, ASTM, Philadelphia, PA.

Barenblatt, G.I. and Joseph, D.D. (1997), *Collected Papers of RS Rivlin*, Springer, New York.

Beatty, M.F. (1987), Topics in Finite Elasticity: Hyperelasticity of Rubber, Elastomers, and Biological Tissues; with examples, **40** 1699-1734.

Begley, M.R. and Mackin, T.J. (2004), Spherical indentation of freestanding circular thin films in the membrane regime, *Journal of the Mechanics and Physics of Solids*. **52**(9), 2005-2023.

Benedict, R., Wineman, A.S. and Yang, W.H. (1979), The determination of limiting pressure in simultaneous elongation and inflation of nonlinear elastic tubes, *International Journal of Solids and Structures*. **15**(3), 241-249.

Blatz, P.J. and Ko, W.L. (1962), Application of finite elastic theory to the deformation of rubbery materials, *Journal of Rheology*. **6** 223-251.

Boyce, M.C. and Arruda, E.M. (2000), Constitutive models of rubber elasticity: a review, *Rubber Chemistry and Technology*. **73** 504-523.

Chen, D. and Cheng, S. (1996), Non-linear analysis of prestretched circular membrane and a modified iteration technique, *International Journal of Solids and Structures*. **33**(4), 545-553.

Christensen, R.M. (1980), A nonlinear theory of viscoelasticity for application to elastomers, *Journal of Applied Mathematics*. **47** 762-768.

Colombi, P. (2006), The ponding problem on flat steel roof grids, *Journal of Constructional Steel Research*. **62**(7), 647-655.

David, G. and Humphrey, J.D. (2004), Redistribution of stress due to a circular hole in a nonlinear anisotropic membrane, *Journal of Biomechanics*. **37**(8), 1197-1203.

Deam, R.T. and Edwards, S.F. (1976), The theory of rubber elasticity, *Philosophical Transactions for the Royal Society of London. Series A, Mathematical and Physical Sciences*. **280** 317-353.

Dickey, R.W. (1967), The plane circular elastic surface under normal pressure, *Archive for Rational Mechanics and Analysis*. **26**(3), 219-236.

Dickey, R.W. (1983), The nonlinear circular membrane under a vertical force, *The Quarterly Journal of Mechanics and Applied Mathematics*. **41** 331-338.

Dong, W. (2006), *Modelling of Advection-Dominated Transport in Fluid-saturated Porous Media*, PhD Thesis, McGill University, Montreal.

Feng, W.W. (1992), Viscoelastic behavior of elastomeric membranes, *Journal of Applied Mechanics*. **59** S29.

Feng, W.W. and Huang, P. (1975), On the general contact problem of an inflated nonlinear plane membrane, *International Journal of Solids and Structures*. **11** 437-448.

Feng, W.W., Tielking, J.T. and Huang, P. (1974), The inflation and contact constraint of a rectangular Mooney membrane, *Journal of Applied Mechanics*. **41** 979-984.

Feng, W.W. and Yang, W.H. (1970), On axisymmetrical deformations of nonlinear membranes, *Journal of Applied Mechanics*. **37** 1002-1011.

Feng, W.W. and Yang, W.H. (1973), On the contact problem of an inflated spherical nonlinear membrane, *Journal of Applied Mechanics*. **40** 209-214.

Feodosev, Y. (1968), On equilibrium modes of a rubber spherical shell under internal pressure, *PMM*. **32** 335-341.

Flory, P.J. and Erman, B. (1982), Theory of elasticity of polymer networks, *Macromolecules*. **15**(3), 800-806.

Gent, A.N. (1996), A new constitutive relation for rubber, *Rubber Chemistry and Technology*. **69**(1), 59-61.

Gent, A.N. (1997). Fracture mechanisms and mechanics, *Elastomer - Finite Element Analysis Forum '97*, University of Akron.

Grabmüller, H. and Novak, E. (1988), Non-linear boundary value problems for the annular membrane: New results on existence of positive solutions, *Mathematical Methods in the Applied Sciences*. **10**(1), 37-49.

Grabmüller, H. and Weinitschke, H.J. (1986), Finite displacements of annular elastic membranes, *Journal of Elasticity*. **16**(2), 135-147.

Green, A.E. and Adkins, J.E. (1970), *Large elastic deformations*, Oxford University Press, London.

Hart-Smith, L.J. (1966), Elasticity parameters for finite deformations of rubber-like materials, *Zeitschrift für Angewandte Mathematik und Physik (ZAMP)*. **17**(5), 608-626.

Hart-Smith, L.J. and Crisp, J.D.C. (1967), Large elastic deformations of thin rubber membranes, *International Journal of Engineering Science*. **5**(1), 1-24.

Hassager, O., Kristensen, S.B., Larsen, J.R. and Neergaard, J. (1999), Inflation and instability of a polymeric membrane, *Journal of Non-Newtonian Fluid Mechanics*. **88**(1-2), 185-204.

Haughton, D.M. (1980), Post-bifurcation of perfect and imperfect spherical elastic membranes, *International Journal of Solids and Structures*. **16**(12), 1123-1134.

Katsikadelis, J.T. and Nerantzaki, M.S. (2002), The ponding problem on elastic membranes: An analog equation solution, *Computational Mechanics*. **28**(2), 122-128.

Katsikadelis, J.T. and Nerantzaki, M.S. (2003), Ponding on floating membranes, *Engineering Analysis with Boundary Elements*. **27**(6), 589-596.

Kelkar, A., Elber, W. and Raju, I.S. (1985), Large deflections of circular isotropic membranes subjected to arbitrary axisymmetric loading, *Computers & Structures*. **21**(3), 413-421.

Khayat, R.E. and Derdouri, A. (1995), Stretch and inflation of hyperelastic membranes as applied to blow moldiing, *Polymer Engineering & Science*. **35**(23), 1852-1863.

Khayat, R.E., Derdouri, A. and Garcia-Rejon, A. (1992), Inflation of an elastic cylindrical membrane: Non-linear deformation and instability, *International Journal of Solids and Structures*. **29**(1), 69-87.

Klingbeil, W.W. and Shield, R.T. (1964), Some numerical investigations on empirical strain energy functions in the large axi-symmetric extensions of rubber membranes, *Zeitschrift für Angewandte Mathematik und Physik (ZAMP)*. **15**(6), 608-629.

Kydoniefs, A.D. and Spencer, A.J.M. (1967), The finite inflation of an elastic toroidal membrane of circular cross section, *International Journal of Engineering Science*. **5** 367-391.

Kydoniefs, A.D. and Spencer, A.J.M. (1969), Finite axisymmetric deformations of an initially cylindrical elastic membrane, *The Quarterly Journal of Mechanics and Applied Mathematics*. **22**(1), 87-95.

Lardner, T.J. and Pujara, P. (1980), Compression of spherical cells, *Mechanics Today*. **5** 161-176.

Li, Y., Nemes, J.A. and Derdouri, A.A. (2001), Membrane inflation of polymeric materials: Experiments and finite element simulations, *Polymer Engineering & Science*. **41**(8), 1399-1412.

Libai, A. and Simmonds, J.G. (1998), *The Nonlinear Theory of Elastic Shells*, Cambridge University Press, Cambridge.

Liu, W. and Rahn, C.R. (2003), Fiber-reinforced membrane models of McKibben actuators, *Journal of Applied Mechanics*. **70**(6), 853-859.

Matsikoudi-Iliopoulou, M. (1987), Finite axisymmetric deformations with torsion of an initially cylindrical membrane reinforced with one family inextensible cords, *International Journal of Engineering Science*. **25**(6), 673-680.

Matsikoudi-Iliopoulou, M. and Lianis, G. (1982), Non linear elastic axisymmetric deformation of membranes with torsion, *Acta Mechanica*. **42**(3), 153-170.

Mooney, M. (1940), A theory of large elastic deformation, *Journal of Applied Physics*. **11** 583-593.

Mori, D., David, G., Humphrey, J.D. and Moore Jr, J.E. (2005), Stress distribution in a circular membrane with a central fixation, *Journal of Biomechanical Engineering*. **127** 549-553.

Müller, I. and Strehlow, P. (2004), *Rubber and Rubber Balloons: Paradigms of Thermodynamics*, Springer, Berlin.

Mullins, L. (1969), Softening of rubber by deformation, *Rubber Chemistry and Technology*. **42** 339-362.

Mullins, L. and Tobin, N.R. (1957), Theoretical model for the elastic behavior of filler-reinforced vulcanized rubbers, *Rubber Chemistry and Technology*. **30** 555-571.

Mullins, L. and Tobin, N.R. (1965), Stress softening in rubber vulcanizates. Part I. Use of a strain amplification factor to describe the elastic behavior of filler-reinforced vulcanized rubber, *Journal of Applied Polymer Science*. **9**(9), 2993-3010.

Needleman, A. (1977), Inflation of spherical rubber balloons, *International Journal of Solids and Structures*. **13**(5), 409-421.

Nerantzaki, M.S. and Kandilas, C.B. (2007), Geometrically nonlinear analysis of elastic membranes with embedded rigid inclusions, *Engineering Analysis with Boundary Elements*. **31**(3), 216-225.

Oden, J.T. and Sato, T. (1967), Finite strains and displacements of elastic membranes by the finite element method, *International Journal of Solids and Structures*. **3** 471-488.

Ogden, R.W. (1972), Large deformation isotropic elasticity-on the correlation of theory and experiment for incompressible rubberlike solids, *Proceedings of the Royal Society of London. Series A, Mathematical and Physical Sciences*. **326** 565-584.

Ogden, R.W. (1982), *Elastic Deformations of Rubberlike Solids*, Pergamon Press, Oxford.

Ogden, R.W. (1984), *Non-Linear Elastic Deformations*, Ellis Horwood, Chichester.

Ogden, R.W. (2004), Elasticity and inelasticity of rubber, *Mechanics and Thermomechanics of Rubberlike Solids*. **452** 135-185.

Przybylo, P.A. and Arruda, E.M. (1998), Experimental investigations and numerical modeling of incompressible elastomers during non-homogeneous deformations, *Rubber Chemistry and Technology*. **71**(4), 730-749.

Rivlin, R.S. (1948), Large elastic deformations of isotropic materials. IV. Further developments of the general theory, *Philosophical Transactions of the Royal Society of London. Series A. Mathematical and Physical Sciences*. **241** 379-397.

Rivlin, R.S. (1960). Some topics in Finite elasticity *Structural Mechanics: Proceedings of the First Symposium on Naval Structural Mechanics*, Oxford.

Saccomandi, G. and Ogden, R.W. (2004), *Mechanics and Thermomechanics of Rubberlike Solids*, Springer, New York.

Scott, O.N., Begley, M.R., Komaragiri, U. and Mackin, T.J. (2004), Indentation of freestanding circular elastomer films using spherical indenters, *Acta Materialia*. **52**(16), 4877-4885.

Selby, J.C. and Shannon, M.A. (2009), Inflation of a circular elastomeric membrane into a horizontally semi-infinite liquid reservoir of finite vertical depth: Quasi-static deformation model *International Journal of Engineering Science*. **47** 700-717.

Selvadurai, A.P.S. (2006), Deflections of a rubber membrane, *Journal of the Mechanics and Physics of Solids*. **54**(6), 1093-1119.

Selvadurai, A.P.S. and Dong, W. (2006), The numerical modelling of advective transport in the presence of fluid pressure transients, *Mechanics of Cohesive-frictional Materials*. **30**(7), 615-634.

Selvadurai, A.P.S. and Yu, Q. (2006), Constitutive modelling of a polymeric material subjected to chemical exposure, *International Journal of Plasticity*. **22**(6), 1089-1122.

Selvadurai, A.P.S. and Yu, Q. (2006), On the indentation of a polymeric membrane, *Proceedings of the Royal Society A: Mathematical, Physical and Engineering Science*. **462**(2065), 189-209.

Shield, R.T. (1972), On the stability of finitely deformed elastic membranes, *Zeitschrift für Angewandte Mathematik und Physik (ZAMP)*. **23**(1), 16-34.

Spencer, A.J.M. (1970), The static theory of finite elasticity, *Journal of Applied Mathematics*. **6**(2), 164-200.

Treloar, L.R.G. (1944), Stress-strain data for vulcanised rubber under various types of deformation, *Transactions of the Faraday Society*. **40** 59-70.

Treloar, L.R.G. (1975), *The Physics of Rubber Elasticity*, Oxford, Clarendon.

Truesdell, C. and Noll, W. (1992), *The Non-Linear Field Theories of Mechanics*, Springer-Verlag, Berlin.

Tuan, C.Y. (1998), Ponding on circular membranes, *International Journal of Solids and Structures*. **35**(3-4), 269-283.

Vaughan, H. (1980), Pressurising a prestretched membrane to form a paraboloid, *International Journal of Engineering Science*. **18**(1), 99-107.

Verron, E., Khayat, R.E., Derdouri, A. and Peseux, B. (1999), Dynamic inflation of hyperelastic spherical membranes, *Journal of Rheology*. **43**(5), 1083-1097.

Weinitschke, H.J. (1980), On axisymmetric deformations of nonlinear elastic membranes, *Mechanics Today*. **5** 523-532.

Weinitschke, H.J. (1987), On finite displacements of circular elastic membranes, *Mathematical Methods in the Applied Sciences*. **9**(1), 76-98.

Wineman, A.S. (1976), Large axisymmetric inflation of a nonlinear viscoelastic membrane by lateral pressure, *Journal of Rheology*. **20** 203-225.

Wineman, A.S. (1978), On axisymmetric deformations of nonlinear viscoelastic membranes, *Journal of Non-Newtonian Fluid Mechanics*. **4**(3), 249-260.

Wineman, A.S. (2007), Nonlinear viscoelastic membranes, *Computers and Mathematics with Applications*. **53**(2), 168-181.

Wineman, A.S., Wilson, D. and Melvin, J.W. (1979), Material identification of soft tissue using membrane inflation, *Journal of Biomechanics*. **12**(11), 841-850.

Wu, C.H. (1971), On the contact problems of inflated cylindrical membranes with a life raft as an example, *Journal of Applied Mechanics*. **38** 615-622.

Yang, W.H. and Lu, C.H. (1973), General deformations of neo-Hookean membranes, *Journal of Applied Mechanics*. **40** 7-12.

Yeoh, O.H. (1993), Some forms of the strain energy function for rubber, *Rubber Chemistry and Technology*. **66**(5), 754-771.

Yeoh, O.H. (1997). A practical guide to rubber constitutive models, *Elastomer - Finite Element Analysis Forum '97*, University of Akron.

Yu, Q. (2005), *The Mechanical Behaviour of Chemically-treated PVC Geosynthetic Membranes*, PhD Thesis, McGill University, Montreal.